iScience

CellPress
OPEN ACCESS

Article

PPARα Ligand-Binding Domain Structures with Endogenous Fatty Acids and Fibrates

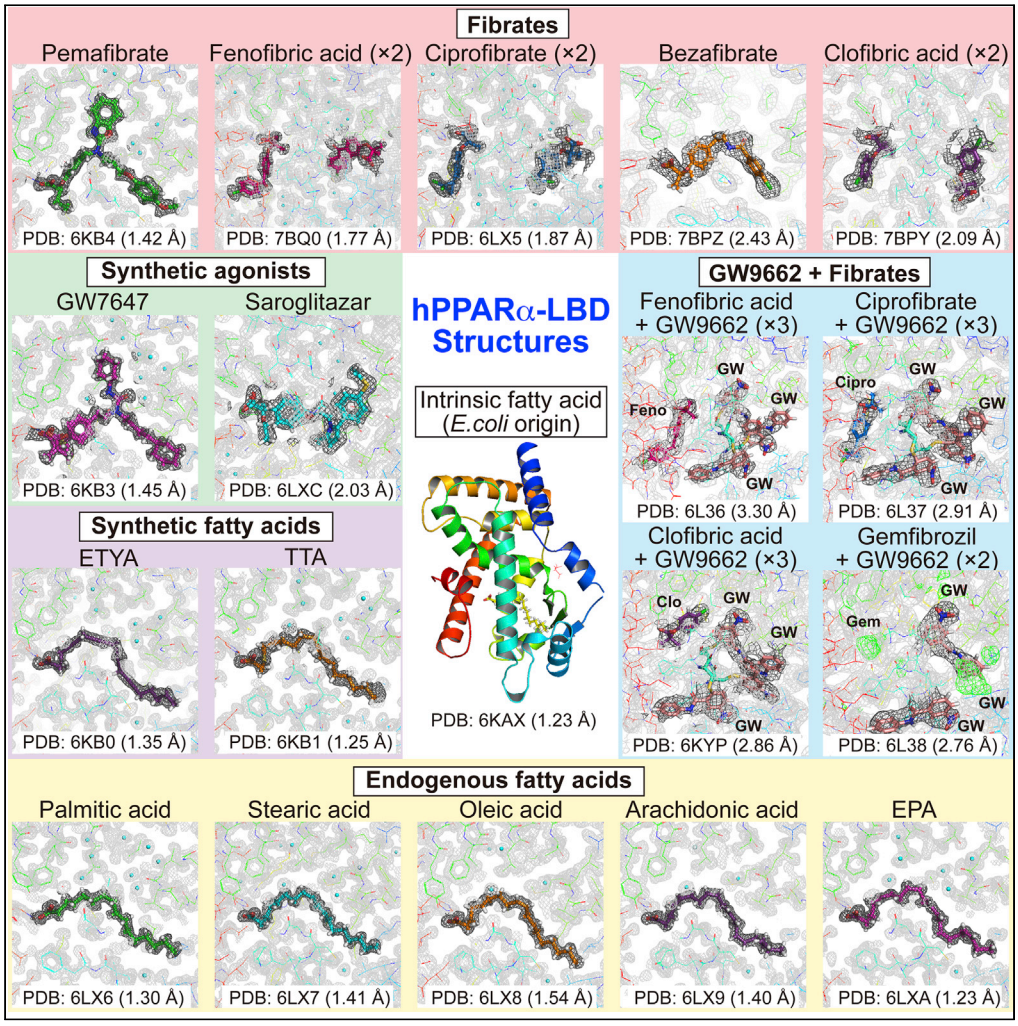

Shotaro Kamata, Takuji Oyama, Kenta Saito, ..., Koji Uchida, Makoto Suematsu, Isao Ishii

isao-ishii@umin.ac.jp

HIGHLIGHTS

X-ray crystallography reveals 34 high-resolution human PPARα-ligand structures

Stearic acid and palmitic acid are presumably physiological PPARα ligands

Coordination to Arm III domain is important for high PPARα potency/selectivity

Agonistic activities of four fibrates are enhanced by the partial agonist GW9662

Kamata et al., iScience 23, 101727
November 20, 2020 © 2020 The Author(s).
https://doi.org/10.1016/j.isci.2020.101727

iScience

CellPress
OPEN ACCESS

Article

PPARα Ligand-Binding Domain Structures with Endogenous Fatty Acids and Fibrates

Shotaro Kamata,[1] Takuji Oyama,[2] Kenta Saito,[1] Akihiro Honda,[1] Yume Yamamoto,[1] Keisuke Suda,[1] Ryo Ishikawa,[1] Toshimasa Itoh,[3] Yasuo Watanabe,[4] Takahiro Shibata,[5] Koji Uchida,[6] Makoto Suematsu,[7] and Isao Ishii[1,8,*]

SUMMARY

Most triacylglycerol-lowering fibrates have been developed in the 1960s–1980s before their molecular target, peroxisome proliferator-activated receptor alpha (PPARα), was identified. Twenty-one ligand-bound PPARα structures have been deposited in the Protein Data Bank since 2001; however, binding modes of fibrates and physiological ligands remain unknown. Here we show thirty-four X-ray crystallographic structures of the PPARα ligand-binding domain, which are composed of a "Center" and four "Arm" regions, in complexes with five endogenous fatty acids, six fibrates in clinical use, and six synthetic PPARα agonists. High-resolution structural analyses, in combination with coactivator recruitment and thermostability assays, demonstrate that stearic and palmitic acids are presumably physiological ligands; coordination to Arm III is important for high PPARα potency/selectivity of pemafibrate and GW7647; and agonistic activities of four fibrates are enhanced by the partial agonist GW9662. These results renew our understanding of PPARα ligand recognition and contribute to the molecular design of next-generation PPAR-targeted drugs.

INTRODUCTION

Cardiovascular diseases (CVDs) have been identified as the leading cause of deaths worldwide, accounting for 17.9 million deaths annually (WHO, 2017). High blood levels of low-density lipoprotein cholesterol (LDL-C), high triacylglycerol (TG), and low high-density lipoprotein cholesterol (HDL-C) are all considered major risk factors for the development of CVD (Andersson et al., 2014). Although statins, which inhibit β-hydroxy-β-methylglutaryl-CoA reductase, are found to lower blood LDL-C levels, fibrates, which are peroxisome proliferator-activated receptor alpha (PPARα) agonists, lower TG levels and elevate HDL-C levels (Bougarne et al., 2018; Yamashita et al., 2019). Combining statins and fibrates could offer therapeutic advantages for the treatment of refractory combined dyslipidemia (Franssen et al., 2009; Han et al., 2017). However, in general, it has not been recommended because of the increased risks of myopathy and rhabdomyolysis (Franssen et al., 2009; Graham et al., 2004).

Differences in the pharmacokinetic interaction potentials of fibrates with statins have emerged (Franssen et al., 2009), which could act on other cognate PPARs (Yamashita et al., 2019), such as PPAR gamma (PPARγ), which regulates lipid/glucose metabolism, mainly in adipose tissue, and is the target of anti-diabetic thiazolidinedione (glitazone) drugs, and PPAR delta (PPARδ), which is expressed in many tissues to govern a variety of biological processes and whose agonists are expected to treat metabolic/cardiovascular diseases (Da'adoosh et al., 2019; Wu et al., 2017). Differential interactions of fibrates with other PPARs could elicit either beneficial effects or undesirable side effects, although novel effects of fibrates, such as synergistic tumor suppression activity with anti-PD-1 antibody (Chamoto et al., 2017), via unknown mechanisms, are also evident. Two PPARα/γ dual agonists, saroglitazar and lobeglitazone, have already been clinically approved in India and Korea, respectively, as next-generation therapeutics for diabetic dyslipidemia (Han et al., 2017). In 2018, pemafibrate, which is also known as K-877 or SPPARMα (selective PPARα modulator), was approved in Japan as a highly PPARα-selective agonist that is safe for simultaneous use with statins, even in patients with mild kidney diseases (Yamashita et al., 2019, 2020; Yokote et al., 2019). Thus, further development of PPAR dual/pan agonists, including PPARα/γ agonists as anti-diabetic drugs (Artis et al., 2009; Bénardeau et al., 2009) and PPARα/δ agonists as anti-nonalcoholic steatohepatitis (NASH) drugs, and PPARα-specific agonists is anticipated (Han et al., 2017).

[1]Laboratory of Health Chemistry, Showa Pharmaceutical University, Machida, Tokyo 194-8543, Japan

[2]Faculty of Life and Environmental Sciences, University of Yamanashi, Kofu, Yamanashi 400-8510, Japan

[3]Laboratory of Drug Design and Medicinal Chemistry, Showa Pharmaceutical University, Machida, Tokyo 194-8543, Japan

[4]Laboratory of Pharmacology, Showa Pharmaceutical University, Machida, Tokyo 194-8543, Japan

[5]Graduate School of Bioagricultural Sciences, Nagoya University, Nagoya, Aichi 464-8601, Japan

[6]Graduate School of Agricultural and Life Sciences, the University of Tokyo, Bunkyo, Tokyo 113-8657, Japan

[7]Department of Biochemistry, Keio University School of Medicine, Shinjuku, Tokyo 160-8582, Japan

[8]Lead Contact

*Correspondence: isao-ishii@umin.ac.jp

https://doi.org/10.1016/j.isci.2020.101727

This is an open access article under the CC BY-NC-ND license (http://creativecommons.org/licenses/by-nc-nd/4.0/).

However, compared with PPARγ and PPARδ, structural information for the PPARα-ligand remains limited. Only 21 records of PPARα structures have been deposited in the Protein Data Bank (PDB; http://www.pdb.org/) (Artis et al., 2009; Bernardes et al., 2013; Bénardeau et al., 2009; Kawasaki et al., 2020; Kuwabara et al., 2012; Oyama et al., 2009; Xu et al., 2001, 2002) (Table S1), in contrast to 224 for PPARγ (Artis et al., 2009; Bénardeau et al., 2009; Brust et al., 2018; Fyffe et al., 2006; Itoh et al., 2008; Kuwabara et al., 2012; Nolte et al., 1998; Oyama et al., 2009) and 44 for PPARδ (Artis et al., 2009; Oyama et al., 2009; Xu et al., 1999). In addition, there have been no depositions for endogenous (physiological) ligands or fibrates, except for pemafibrate (Kawasaki et al., 2020). The limited data describe the 1,400 $Å^3$ cavity of the PPARα-ligand-binding domain (LBD) (Xu et al., 2001), which is equivalent to the PPARγ-LBD (1,440 $Å^3$) and PPARδ-LBD (1,300 $Å^3$) but is found much larger than those observed in other nuclear receptors (600–1,100 $Å^3$) (Itoh et al., 2008; Wu et al., 2017; Xu et al., 1999). It is composed of five regions; Arm I, which is surrounded by helices 3, 11, and 12 and loop H11–H12; Arm II, with helices 2′ and 3 and strands 1, 3, 4; Arm III, with helices 3 and 5 and loop H1–H2; Arm X, which is outside of Arm II; and Center, with helices 3, 5, 7, and 12 (which we renamed from Zoete et al., 2007; Figure S1). However, the roles of those regions for fibrate recognition are yet to be determined.

Using X-ray crystallography, this study provided 34 high-resolution PPARα-LBD structures in complexes with 17 ligands (Figure S2), which include endogenous fatty acids, all clinically approved fibrates, and other synthetic PPARα agonists (Han et al., 2017). Although the study was underway, Kawasaki et al. (2020) reported an X-ray crystal structure of the ternary complex of PPARα-LBD/pemafibrate/coactivator peptide at 3.20 Å resolution (1.52 Å in this study), in which quite limited information was available about the location of pemafibrate and its surrounding amino acid side chains.

RESULTS

Structures with Intrinsic Fatty Acids

Unlike PPARγ (Nolte et al., 1998), it was difficult to obtain PPARα apocrystals. First, we reproduced Wy14643-bound crystals (Bernardes et al., 2013) using co-crystallization (Hassell et al., 2007) with highly purified human PPARα-LBD recombinant proteins (Oyama et al., 2009; Capelli et al., 2016) (Figures S3A–S3C). The Wy14643-bound rod-shaped crystals (Figure 1A) that we formed using buffer no. 43 of the Index kit (Table S2, related to Figure 1) provided similar but higher-resolution (1.82 Å) diffraction data, including its two binding sites in Center with Arm X, than the referenced report (Bernardes et al., 2013) (Figures S4A and S4B). Collected crystallography data and refinement statistics (Tables S3 and S4) were deposited in the PDB. Next, we used cross-seeding (Hassell et al., 2007) to obtain crystals containing an intrinsic fatty acid (iFA) of *Escherichia coli* origin (Figure 1A) from crushes of the Wy14643-bound crystals as crystal nuclei (Benvenuti et al., 2007) (Figure S3C), which gave an atomic resolution (1.23 Å) data (Figures 1B and 1C). The *Fo-Fc* omit map illustrated the electron density of palmitic acid, stearic acid, oleic acid, or vaccenic acid (18:1, *trans*-11 (n–7) that is most abundant in *E. coli* extracts (Fyffe et al., 2006)) (Figure 1C). Mass spectrometry analyses of the lipid contents of PPARα-LBD proteins showed that they are mixtures of palmitic acid, stearic acid, and oleic or vaccenic acid, which is difficult to distinguish when using mass spectrometry (Figure 1D). Among these, palmitic acid and stearic acid displayed PPARγ coactivator 1-alpha (PGC1α) coactivator recruitment activity as a measure of PPARα activation (Figure 1E). When five young male undergraduate student volunteers were fasted for 12 h, their serum-free fatty acid concentrations were 114, 48, 133, and 78 μM for palmitic, stearic, oleic, and linoleic acid, respectively. When they were fed thereafter, these concentrations were dramatically declined to 41, 21, 17, and 7 μM, respectively, after 2 h (Figure 1F). Stearic acid (45 μM) and, more potently, its combination with palmitic acid (110 μM) significantly activated PPARα, but further supplementation of oleic acid (130 μM) plus linoleic acid (75 μM) abolished it (Figure 1G). A thermostability assay also identified higher Tm values in stearic and palmitic acids rather than in oleic acid (Figure 1I). These data suggest that both stearic and palmitic acids are physiological PPARα ligands. Their potency for PPARα activation/stabilization was lower than most synthetic PPARα agonists but equivalent to clofibric acid and higher than gemfibrozil (Figures 1H and 1I). The pharmacological effects of fibrates in clinical use are elicited by their replacement with iFAs in the PPARα-LBD.

Structures with Various PPARα Agonists

By using the soaking method (Hassell et al., 2007; Kuwabara et al., 2012) (Figure S3C), we were able to obtain crystals with potent agonists; pemafibrate, GW7647, 5,8,11,14-eicosatetraynoic acid (ETYA), sarogliTazar, tetradecylthioacetic acid (TTA), and Wy14643 for high-resolution crystallography (Figures 2A and S4C). Crystals with pemafibrate and GW7647 were also acquired through cross-seeding (Figure 2B).

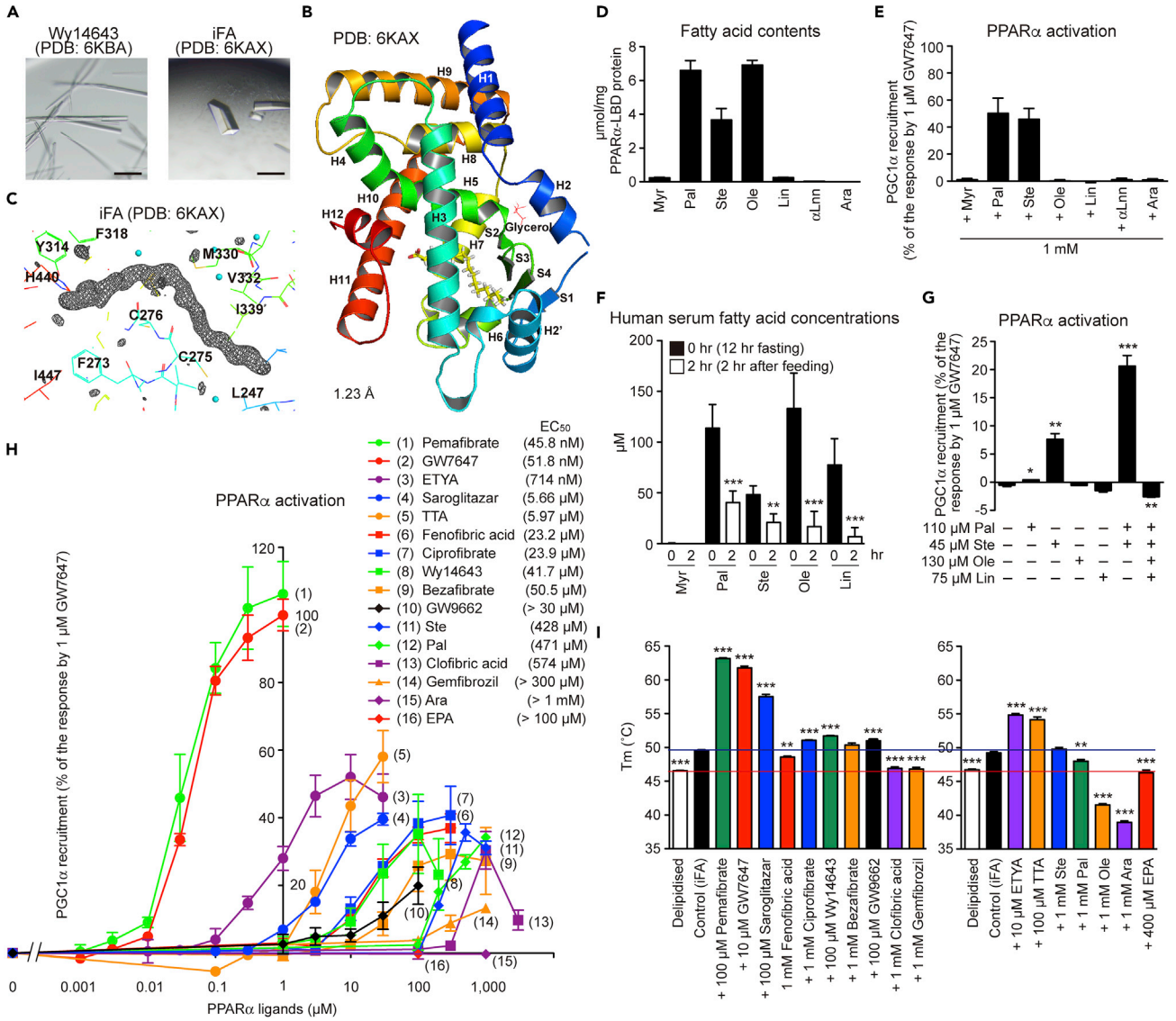

Figure 1. Structures of Intrinsic Fatty Acid-Bound PPARα-LBD and PPARα Activation by Endogenous Fatty Acids

(A) Intrinsic fatty acid (iFA)-bound crystals (*right*) obtained using crushed Wy14643-bound crystals (*left*) as crystal nuclei. Scale bars: 100 μm.

(B) High-resolution (1.23 Å) structure of PPARα-LBD and iFA (yellow). α-helices, β-sheets, and glycerol are labeled.

(C) Magnified view of iFA and surrounding amino acids. The electron density is shown in the mesh by *Fo-Fc* omit map contoured at 3.0σ. Water molecules are presented as cyan spheres.

(D) Contents of the seven major fatty acids (of *E. coli* origin) in PPARα-LBD proteins measured by LC-MS/MS analysis.

(E) PPARα activation (PGC1α coactivator recruitment) by endogenous fatty acids. Maximal response by 1 μM GW7647 was set as 100 (%).

(F) Serum fatty acid contents of five healthy male volunteers who were fasted for 12 h and then fed. Serum fatty acid levels were decreased after 2 h.

(G) Effects of fatty acid combinations on PPARα activation.

(H) Concentration-dependent PPARα activation by several ligands; their EC50 values are shown in parentheses.

(I) Effects of several ligands on PPARα-LBD thermostability. Ligands were dissolved in 100% DMSO (*left*) or 100% ethanol (*right*), and their final concentrations in assays were 0.1%.

The differences versus control (0 h in (F), no lipids in (G), and iFA-bound proteins in (I)) are significant at *$p < 0.05$, **$p < 0.01$, and ***$p < 0.001$. Data are means ± SEM in (D) ($n = 3$), (E) ($n = 3$), (G) ($n = 4$), (H) ($n = 3$–4), and (I) ($n = 4$–6), and means ± SD in (F) ($n = 5$). Myr, myristic acid; Pal, palmitic acid; Ste, stearic acid; Ole, oleic acid; Lin, linoleic acid; αLnn, α-linolenic acid; and Ara, arachidonic acid.

Because we failed to obtain crystals with less potent agonists, iFAs were removed using delipidation (Figure S3D) in order to obtain apoproteins. The delipidized PPARα-LBD protein preserved its molecular weight, but ~80% of the protein lost its iFAs (Figures S3E and S3F). The delipidation induced a slight shift

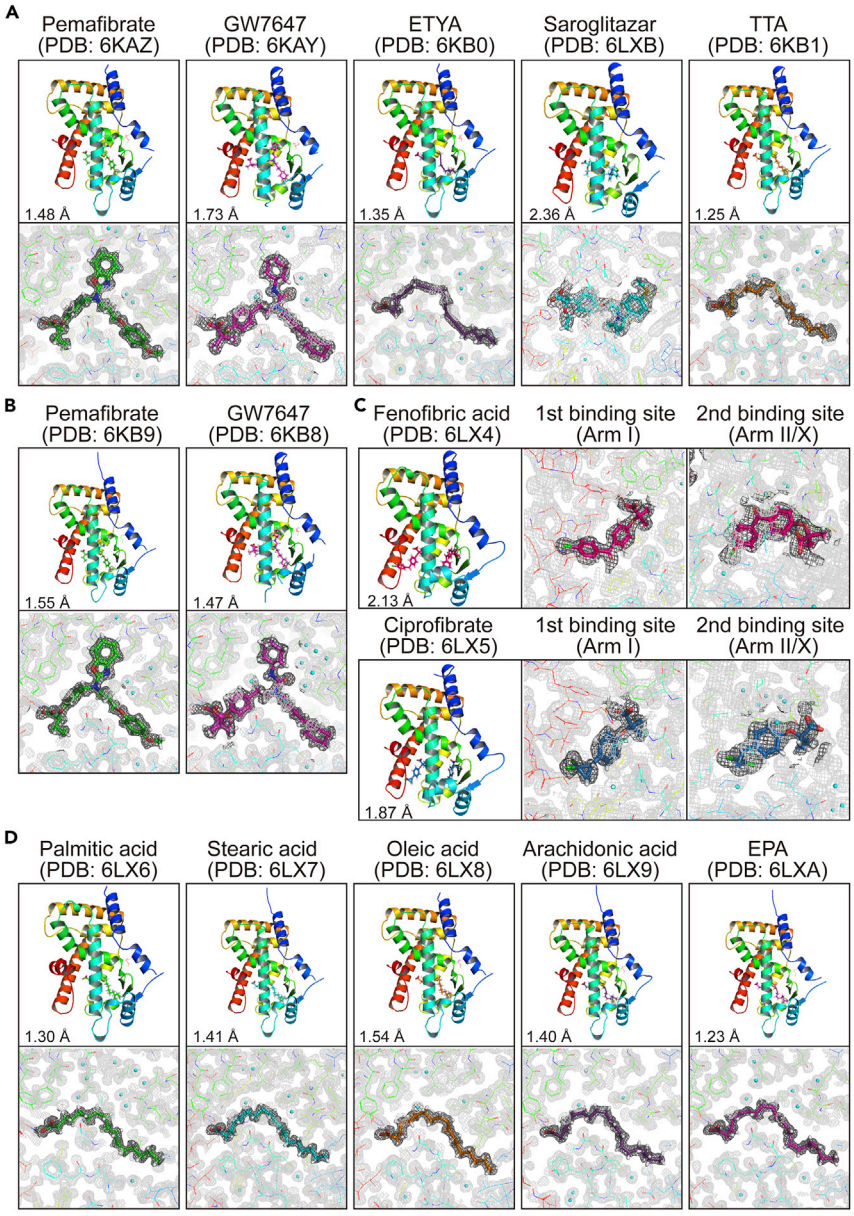

Figure 2. PPARα-LBD-ligand Structures Obtained Using Soaking, Cross-Seeding, and Delipidation Methods for Crystallization

(A–D) Crystal structures and magnified views of PPARα-LBD and five potent PPARα agonists obtained using soaking (A); two potent PPARα agonists obtained using cross-seeding (see also Figure S5) (B); two intermediately potent PPARα agonists obtained using co-crystallization of the delipidized proteins (C); or five exogenous fatty acids with relatively low potency obtained by cross-seeding of the delipidized proteins (D).

The electron density is shown in the mesh by Feature Enhanced Maps (FEMs) contoured at 1.0σ. PDB identities and resolutions are labeled, and water molecules are presented as cyan spheres.

in the circular dichroism (CD) spectrum from its original protein, but this was restored using stearic acid (1 mM) supplementation (Figure S3G). The delipidized protein displayed ligand concentration-dependent PPARα activation (Figure S3H). Therefore, the delipidation was able to maintain PPARα activity. We also obtained crystals of the delipidized proteins bound with fenofibric acid, ciprofibrate (Figure 2C), five endogenous fatty acids (Figure 2D), and other synthetic ligands (Figures S4D and S5). Importantly, PPAR-α-LBD-ligand structures were conserved in crystals formed by different methods. The coordination of some ligands to PPARα-LBD was independently supported by anomalous dispersion signals from low Z-atoms of

sulfur (in ligands or surrounding Met/Cys residues of proteins) and chloride (in ligands). Anomalous difference Fourier maps, which were obtained using 1.8 Å X-ray, detected sulfur signals from Wy14643, GW7647, saroglitazar, and TTA, as well as chloride signals from fenofibric acid and ciprofibrate, in the exact positions that conventional 1.0 Å X-ray crystallography was deployed (Figure S6).

Ternary Complex with Ligands and Coactivators

Activation Function-2 (AF-2) helix 12 is known to form in the active PPAR conformation (Xu et al., 2002; Zoete et al., 2007). Coexistence with coactivator peptides could enhance PPARα-ligand complex stability through interaction with the AF-2 helix 12 and thereby facilitate crystal formation (Kawasaki et al., 2020; Xu et al., 2001). Indeed, among the 21 structures deposited in PDB (Table S1), 12 structures were obtained with any coactivator: 8 with steroid receptor coactivator-1 (SRC1), 2 with PGC1α, 1 with PPARγ coactivator 1-beta, and 1 with the silencing mediator of retinoic acid and thyroid hormone receptors. Therefore, we produced crystals with a SRC1 peptide. First, we were able to obtain crystals of the ternary complex with an iFA, GW7647, and eicosapentaenoic acid (EPA) using co-crystallization (Figure 3A) and then with pemafibrate by soaking with the PPARα-LBD-iFA-SRC1 cocrystals (Figure 3B). We were also able to obtain structures with clofibric acid and fenofibric acid using co-crystallization with the delipidized protein, in which both fibrates have two binding sites in Arm I and Arm II/X boundary (Figure 3C), and then with bezafibrate by soaking with the PPARα-LBD-clofibric acid-SRC1 cocrystals (Figure 3D). In all cases, SRC1 peptides were associated with helix 12 in a similar manner (Figure 3). We examined molecular interactions between amino acid residues of PPARα-LBD and ligands using LigPlot + analysis (Figure S7). All 15 ligands have a single carboxylic acid surrounded by common residues (S280, Y314, H440, and Y464) located between Arm I and Center regions. Most of the interactions between ligands and amino acid residues, except carboxylic acids, were found to be hydrophobic rather than electrostatic. The location of the first fenofibric acid, ciprofibrate, and clofibric acid molecules in Arm I might flip the neighboring benzyl side chains of Phe273 and the presence of the second those molecules in Arm X could affect the orientation of the helices 2′ (Figures 2C, 3C, and S7), which may affect PPARα activation. Pemafibrate and GW7647 in Arm III might interact with Thr279 via their hydrogen bonds (a water molecule mediated in case of GW7647), thereby stabilizing the helix 3 and the coactivator binding pocket (Figures 2A, 2B, 3A, 3B, and S7).

Bilateral Effects of GW9662

The PPARγ-selective antagonist GW9662 is considered unique because it covalently cross-links with Cys285 of PPARγ-LBD, which is equivalent to Cys276 in the Center region of PPARα-LBD (Brust et al., 2018), and acts as both an agonist and antagonist against PPARα, whereas it is only antagonistic against PPARγ and PPARδ (Leesnitzer et al., 2002). Indeed, we observed that GW9662 inhibits PPARα activation by potent agonists, such as pemafibrate, GW7647, ETYA, and TTA, whereas it enhances activation by less potent agonists: fenofibric acid, ciprofibrate, clofibric acid, and gemfibrozil (Figure 4A). Furthermore, a thermostability assay has showed that GW9662 lowers the PPARα-LBD stability induced by pemafibrate, GW7647, ETYA, saroglitazar, and TTA, whereas it enhances that induced by fenofibric acid, ciprofibrate, Wy14643, bezafibrate, clofibric acid, and gemfibrozil (Figure 4B). We analyzed the cocrystals with GW9662 and fibrates: fenofibric acid, ciprofibrate, clofibric acid, and gemfibrozil (Figures 4C and S8A). The second molecules of the first three fibrates located at Arm II/X were replaced by three GW9662 molecules via their covalent cross-linking to Cys275/Cys278 in Arm X and Cys276 in Arm II (Figures S8A and S8B). Cross-linking to Cys276 rather than Cys275 was important for both the inhibitory effects and enhancing effects (Figure 4D). We were not able to obtain crystals with gemfibrozil but only those bound with both gemfibrozil and GW9662 (Figure S8A). Although the electron density images of gemfibrozil in Arm I and GW9662, which was bound to Cys275, in Arm X were not clear, two GW9662 molecules were cross-linked to Cys276 in Arm II and Cys278 in Arm X. As GW9662 enhanced gemfibrozil-induced PPARα activation/thermostability (Figures 4A and 4B), gemfibrozil may have the second binding site in Arm II/X, besides the Arm I/Center region, like other fibrates (Figure 4E).

DISCUSSION

The transcription factor/nuclear receptor PPARα is a master regulator of lipid metabolism (or metabolism in general) that is activated upon fasting in liver and other tissues and regulates the expression of hundreds of genes involved in lipid (/glucose/amino acid) metabolism as well as biotransformation and inflammation (Rakhshandehroo et al., 2010; Kamata et al., 2018). This study has demonstrated thirty-four structures of human PPARα-LBD with seventeen ligands (and a coactivator) (Table 1), highlighting its versatile recognition

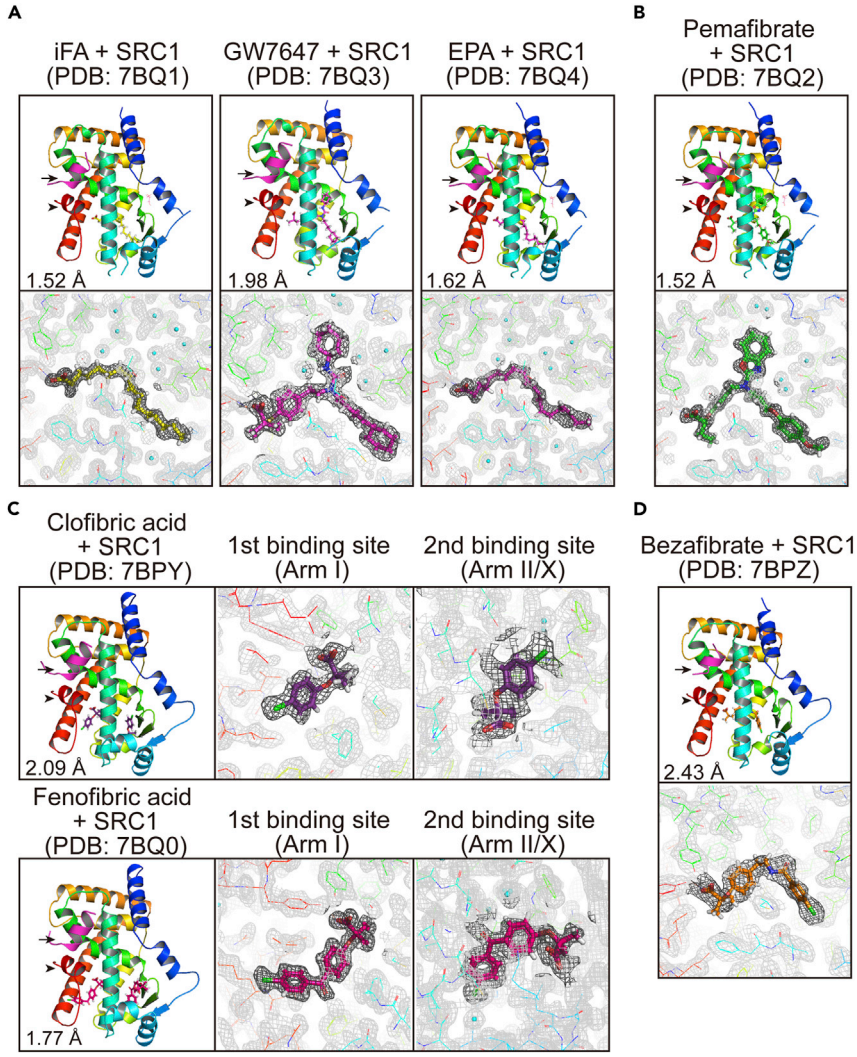

Figure 3. Crystal Structures of Ternary Complexes of PPARα-LBD, Ligand, and SRC1 Coactivator Peptide

(A) Ternary complexes with intrinsic fatty acid (iFA), GW7647, or EPA obtained by co-crystallization.

(B) Ternary complexes with pemafibrate obtained using soaking with iFA/SRC1-bound crystals.

(C) Ternary complexes with clofibric acid or fenofibric acid obtained by co-crystallization of the delipidized proteins. Both fibrates have two binding sites in Arm I and Arm II/X.

(D) Ternary complexes with bezafibrate obtained by soaking with clofibric acid/SRC1-bound crystals.

SRC1 peptides (*magenta*) and helices 12 (*red*) are indicated by arrows and arrowheads. The electron density is shown in the mesh by FEMs contoured at 1.0σ. PDB identities and resolutions are labeled, and water molecules are presented as cyan spheres.

of those ligands (Figure 4E). Among several endogenous PPARα ligand fatty acid candidates (Han et al., 2017), stearic acid and palmitic acid, the prevalent fatty acids released to bloodstream from cellular TG stores upon fasting (Figure 1F), have been found to bind to and activate PPARα (Figures 2D and 1G) for the integral control of lipid metabolism. Meanwhile, oleic acid, arachidonic acid, and EPA could bind to PPARα-LBD and form helix 12 (a hallmark of PPAR activation) (Figure 2D) but not activate it (Figure 1H). Although the helix 12 structure-function model has been popular in the nuclear receptor field, it is challenged by a new concept that agonists with graded activity display gradations in their ability to stabilize the LBD (Kojetin and Burris, 2013); as for PPARγ, in particular on helix 3, 11, and 12, all in a manner that correlates with the graded response of the ligand (Bruning et al., 2007). Therefore, the further experiments utilizing amide H/D exchange or paramagnetic relaxation enhancement NMR may reveal differences in the PPARα-LBD stability induced by those fatty acids. Although *in vitro* binding experiments suggest that

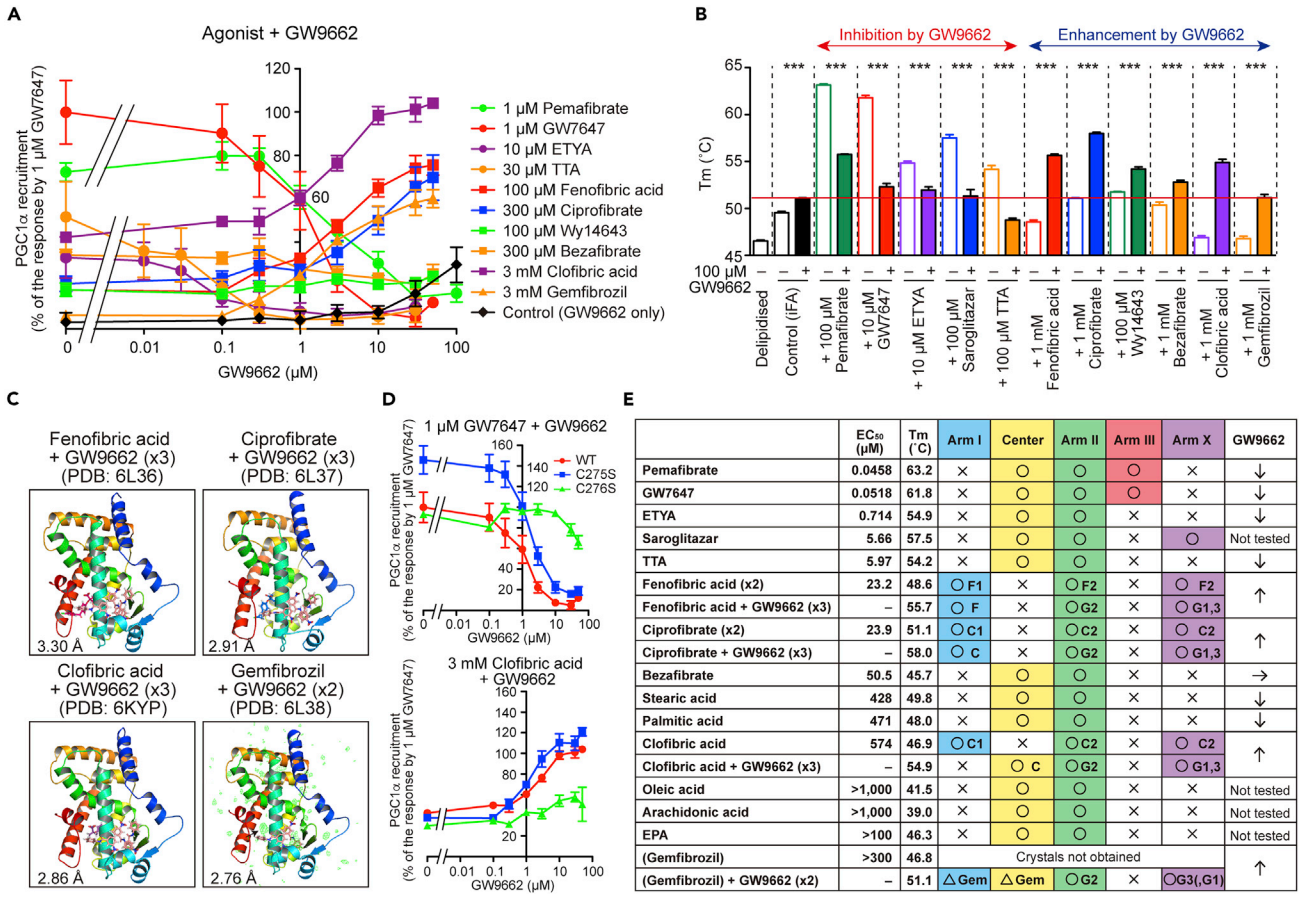

E

	EC_{50} (μM)	Tm (°C)	Arm I	Center	Arm II	Arm III	Arm X	GW9662
Pemafibrate	0.0458	63.2	×	○	○	○	×	↓
GW7647	0.0518	61.8	×	○	○	○	×	↓
ETYA	0.714	54.9	×	○	○	×	×	↓
Saroglitazar	5.66	57.5	×	○	○	×	○	Not tested
TTA	5.97	54.2	×	○	○	×	×	↓
Fenofibric acid (x2)	23.2	48.6	○ F1	×	○ F2	×	○ F2	↑
Fenofibric acid + GW9662 (x3)	–	55.7	○ F	×	○ G2	×	○ G1,3	
Ciprofibrate (x2)	23.9	51.1	○ C1	×	○ C2	×	○ C2	↑
Ciprofibrate + GW9662 (x3)	–	58.0	○ C	×	○ G2	×	○ G1,3	
Bezafibrate	50.5	45.7	×	○	○	×	×	→
Stearic acid	428	49.8	×	○	○	×	×	↓
Palmitic acid	471	48.0	×	○	○	×	×	↓
Clofibric acid	574	46.9	○ C1	×	○ C2	×	○ C2	↑
Clofibric acid + GW9662 (x3)	–	54.9	×	○ C	○ G2	×	○ G1,3	
Oleic acid	>1,000	41.5	×	○	○	×	×	Not tested
Arachidonic acid	>1,000	39.0	×	○	○	×	×	Not tested
EPA	>100	46.3	×	○	○	×	×	Not tested
(Gemfibrozil)	>300	46.8	Crystals not obtained					↑
(Gemfibrozil) + GW9662 (x2)	–	51.1	△ Gem	△ Gem	○ G2	×	○ G3(,G1)	

Figure 4. Structural Basis for Bilateral Effects of GW9662 in PPARα Activation

(A) Concentration-dependent bilateral effects of GW9662 on PGC1α recruitment by agonists with various potencies. Data are means ± SEM (n = 3–4).

(B) Bilateral effects of GW9662 (100 μM) on ligand-induced PPARα-LBD thermostability. Data are means ± SEM (n = 3–4) and effects are found to be significant at ***$p < 0.001$.

(C) Crystal structures of PPARα-LBD bound with single fibrate and two or three GW9662 molecules. See also Figure S8.

(D) Covalent cross-linking to Cys 276, in Arm II, but not to Cys 275, in Arm X, is essential for bilateral effects of GW9662 on PPARα regulation to inhibit GW7647 effects and activate clofibric acid effects. Data are means ± SEM (n = 3).

(E) Summary of bilateral effects of GW9662 and alignment of 16 ligands to LBD pockets in the order of ligand potencies in the coactivator recruitment assay; ligand-induced thermostability data were attached. Structural analyses demonstrated the location (circles), the possible location (triangles), or the absence (crosses) of those ligands in each LBD. One fenofibric acid (F) molecule is located at Arm I (as F1), whereas another fenofibric acid molecule is located across Arms II and X (as F2), and the same applies for GW9662, ciprofibrate, clofibric acid, and gemfibrozil.

multiple endogenous fatty acids could bind to PPARα/γ/δ-LBD (Xu et al., 1999), only oleic acid and arachidonic acid were found to be bound to PPARγ-LBD (Shang et al., 2018) and EPA to PPARδ-LBD (Xu et al., 1999) in X-ray crystallography, in addition to our PPARα-LBD analyses in this study. It is notable that oleic acid and arachidonic acid were found to bind to almost identical loci of PPARα-LBD (Figure 2D) but to different loci of PPARγ-LBD (Shang et al., 2018). EPA was also bound to different loci of PPARα-LBD (Figure 2D) and PPARδ-LBD (Xu et al., 1999).

We also revealed PPARα-LBD structures with all six fibrates in clinical use. Although fibrates are less popular than statins as anti-dyslipidemia drugs in most countries including Japan, the occurrence of fibrates and their metabolites in source and drinking water was reported in China and other countries (Ido et al., 2017) and the world recipient population is estimated to be huge. Therefore, our findings will attract over millions of patients who take fibrates and doctors who prescribe them. As Bernardes et al. (2013) reported with Wy14643-bound crystals, fenofibric acid, ciprofibrate, clofibric acid, and, perhaps, gemfibrozil, have been found to possess two binding sites. Moreover, single fibrates, fenofibric acid, ciprofibrate, and clofibric acid and three GW9662 could occupy PPARα-LBD at the same time, and the PPARα-LBD cavity was

No.	PDB ID	Resolution (Å)	Ligand(s) (±SRC1)	Methods	Deposited Date
1	6KAX	1.23	Intrinsic fatty acid	Cross-seeding	2019/6/24
23	6LXA	1.23	EPA	Delipidation/cross-seeding	2020/2/10
10	6KB1	1.25	TTA	Soaking	2019/6/24
19	6LX6	1.30	Palmitic acid	Delipidation/cross-seeding	2020/2/10
8	6KB0	1.35	ETYA	Soaking	2019/6/24
22	6LX9	1.40	Arachidonic acid	Delipidation/cross-seeding	2020/2/10
20	6LX7	1.41	Stearic acid	Delipidation/cross-seeding	2020/2/10
4	6KB4	1.42	Pemafibrate	Delipidation/cross-seeding	2019/6/24
11	6KB6	1.43	TTA	Delipidation/cross-seeding	2019/6/24
7	6KB3	1.45	GW7647	Delipidation/cross-seeding	2019/6/24
6	6KB8	1.47	GW7647	Cross-seeding	2019/6/24
2	6KAZ	1.48	Pemafibrate	Soaking	2019/6/24
32	7BQ2	1.52	Pemafibrate + SRC1	Soaking (in no.31 crystals)	2020/3/23
31	7BQ1	1.52	iFA + SRC1	Co-crystallization	2020/3/23
21	6LX8	1.54	Oleic acid	Delipidation/cross-seeding	2020/2/10
3	6KB9	1.55	Pemafibrate	Cross-seeding	2019/6/24
34	7BQ4	1.62	EPA + SRC1	Delipidation/co-crystallization	2020/3/23
5	6KAY	1.73	GW7647	Soaking	2019/6/24
30	7BQ0	1.77	Fenofibric acid + SRC1	Delipidation/co-crystallization	2020/3/23
15	6KBA	1.82	Wy14643	Co-crystallization	2019/6/24
18	6LX5	1.87	Ciprofibrate	Delipidation/co-crystallization	2020/2/10
14	6KB2	1.95	Wy14643	Soaking	2019/6/24
9	6KB5	1.95	ETYA	Delipidation/cross-seeding	2019/6/24
33	7BQ3	1.98	GW7647 + SRC1	Delipidation/co-crystallization	2020/3/23
13	6LXC	2.03	Saroglitazar	Delipidation/cross-seeding	2020/2/10
28	7BPY	2.09	Clofibric acid + SRC1	Delipidation/co-crystallization	2020/3/23
17	6LX4	2.13	Fenofibric acid	Delipidation/co-crystallization	2020/2/10
16	6KB7	2.14	Wy14643	Delipidation/cross-seeding	2019/6/24
12	6LXB	2.36	Saroglitazar	Soaking	2020/2/10
29	7BPZ	2.43	Bezafibrate + SRC1	Soaking (in no.28 crystals)	2020/3/23

Table 1. Thirty-Four PPARα-LBD Crystal Structures Newly Deposited in the Protein Data Bank (PDB) from This Study

(Continued on next page)

No.	PDB ID	Resolution (Å)	Ligand(s) (±SRC1)	Methods	Deposited Date
27	6L38	2.76	GW9662 + Gemfibrozil	Delipidation/co-crystallization	2019/10/9
24	6KYP	2.86	GW9662 + Clofibric acid	Delipidation/co-crystallization	2019/9/19
26	6L37	2.91	GW9662 + Ciprofibrate	Delipidation/co-crystallization	2019/10/9
25	6L36	3.30	GW9662 + Fenofibric acid	Delipidation/co-crystallization	2019/10/9

Table 1. Continued

Data are ordered by resolution, and crystal numbers (no.) are identical to those in Tables S3 and S4. No.1 crystals were used as a common seed for cross-seeding and as an original crystal in soaking except for nos. 29 and 32. Nos. 28 and 31 crystals were used in soaking for nos. 29 and 32, respectively. Delipidized proteins were used for co-crystallization in delipidation. SRC1 is a PPARα coactivator peptide.

determined to be large enough to accept multiple ligands with various structures (Figure S8C). Among them, the coordination to Arm III and carboxylic acid-binding site is a key for the highest PPARα activity/selectivity. Molecular extension into the greater depth of Arm III deserves consideration for PPARα-selective agonists, and effective utilization of the other spaces, even by multiple same or different ligands, may be important for the development of more potent PPARα agonists. Furthermore, the precise structure comparison analyses of human PPARα/γ/δ-LBD contributes to the development of new PPAR dual/pan agonists as next-generation metabolic disease drugs. Finally, all previously deposited PPARα-LBD X-ray crystal structures except PDB 1KKQ are the ligand-bound active forms (Table S1) and all 34 structures obtained in this study (Table 1) are also the ligand-bound active forms with helix 12. The high-resolution PPARα-LBD structures that we provided here may help the design of high-affinity PPARα antagonists that stabilize the inactive form (with a corepressor).

Limitations of the Study

The coactivator recruitment and thermostability assays demonstrated graded responses (in efficacy and potency) between several PPARα ligands; however, the thirty-four PPARα-LBD-ligand structures we obtained were all similar activated forms. The amide H/D exchange or paramagnetic relaxation enhancement NMR could detect differences in the PPARα-LBD-ligand stability, and the cryogenic electron microscopy might reveal altered PPARα-LBD structures depending on the ligands. The acquisition of structures of PPARα-LBD inactivated forms is awaited.

Resource Availability

Lead Contact

Further information and requests for resources and reagents should be directed to and will be fulfilled by the Lead Contact, Isao Ishii (isao-ishii@umin.ac.jp).

Materials Availability

This study did not generate new unique reagents.

Data and Code Availability

The data supporting the findings of this study is available within this paper and its Supplemental Information. PDB IDs for the 34 PPARα-ligand structures reported in this paper are: 6KAX (intrinsic fatty acid); 6KAZ, 6KB9, 6KB4 (pemafibrate); 6KAY, 6KB8, 6KB3 (GW7647); 6KB0, 6KB5 (ETYA); 6KB1, 6KB6 (TTA); 6KXB, 6LXC (saroglotazar); 6KB2, 6KBA, 6KB7 (Wy14643); 6LX4 (fenofibric acid); 6LX5 (ciprofibrate); 6LX6 (palmitic acid); 6LX7 (stearic acid); 6LXB8 (oleic acid); 6LX9 (arachidonic acid); 6LXA (EPA); 6KYP (GW9662 + clofibric acid); 6L36 (GW9662 + fenofibric acid); 6L37 (GW9662 + ciprofibrate); 6L38 (GW9662 + gemfibrozil); 7BPY (clofibric acid + SRC1); 7BPZ (bezafibrate + SRC1); 7BQ0 (fenofibric acid + SRC1); 7BQ1 (intrinsic fatty acid + SRC1); 7BQ2 (pemafibrate + SRC1); 7BQ3 (GW7647 + SRC1); and 7BQ4 (EPA + SRC1).

METHODS

All methods can be found in the accompanying Transparent Methods supplemental file.

SUPPLEMENTAL INFORMATION

Supplemental Information can be found online at https://doi.org/10.1016/j.isci.2020.101727.

ACKNOWLEDGMENTS

We thank Prof. Jerold Chun (Sanford Burnham Prebys Medical Discovery Institute) for helpful comments. S.K. and I.I. acknowledge fundings from Grants-in-Aid for Scientific Research from Japan Society for the Promotion of Sciences (JSPS), Japan (grant numbers: 19K16359 and 16H05107), Platform Project for Supporting Drug Discovery and Life Science Research (Basis for Supporting Innovative Drug Discovery and Life Science Research [BINDS]) from AMED, Japan (grant number: JP19am0101071; support number: 1407), and Showa Pharmaceutical University, Japan. T.O. acknowledges fundings from a Grant-in-Aid for Scientific Research from JSPS (grant number: 18K06081) and Adaptable and Seamless Technology Transfer Program through Target-driven R&D (A-STEP) from Japan Science and Technology Agency, Japan (grant number: JPMJTM19AT). This work was performed under the approval of the Photon Factory Program Advisory Committee, Japan (proposal number: 2018G658).

AUTHOR CONTRIBUTIONS

S.K., T.O., and I.I. conceived the study. S.K., T.O., K. Saito, A.H., K. Suda, and T.I. preformed crystal preparation and X-ray crystallography. S.K. and I.I. deposited all PDB data. S.K., A.H., and Y.Y. performed TR-FRET assay. S.K. and A.H. performed CD spectrometry. S.K., T.O., K. Saito, R.I., and T.I. performed crystal structure analyses. Y.W. performed blood drawing. T.S. and K.U. performed lipid analyses. S.K., T.O., K.S., A.H., T.I., Y.W., M.S., and I.I. interpreted data. T.O. and I.I. supervised the study. I.I. wrote the paper, with input from all authors.

DECLARATION OF INTERESTS

The authors declare no competing interest.

Received: September 11, 2020
Revised: October 8, 2020
Accepted: October 20, 2020
Published: November 20, 2020

REFERENCES

Andersson, C., Lyass, A., Vasan, R.S., Massaro, J.M., D'Agostino, R.B. Sr, and Robins, S.J. (2014). Long-term risk of cardiovascular events across a spectrum of adverse major plasma lipid combinations in the Framingham Heart Study. Am. Heart J. *168*, 878–883.e1.

Artis, D.R., Lin, J.J., Zhang, C., Wang, W., Mehra, U., Perreault, M., Erbe, D., Krupka, H.I., England, B.P., Arnold, J., et al. (2009). Scaffold-based discovery of indeglitazar, a PPAR pan-active anti-diabetic agent. Proc. Natl. Acad. Sci. U S A *106*, 262–267.

Bénardeau, A., Benz, J., Binggeli, A., Blum, D., Boehringer, M., Grether, U., Hilpert, H., Kuhn, B., Märki, H.P., Meyer, M., et al. (2009). Aleglitazar, a new, potent, and balanced dual PPARalpha/gamma agonist for the treatment of type II diabetes. Bioorg. Med. Chem. Lett. *19*, 2468–2473.

Benvenuti, M., and Mangani, S. (2007). Crystallization of soluble proteins in vapor diffusion for x-ray crystallography. Nat. Protoc. *2*, 1633–1651.

Bernardes, A., Souza, P.C., Muniz, J.R., Ricci, C.G., Ayers, S.D., Parekh, N.M., Godoy, A.S., Trivella, D.B., Reinach, P., Webb, P., et al. (2013). Molecular mechanism of peroxisome proliferator-activated receptor alpha activation by WY14643: a new mode of ligand recognition and receptor stabilization. J. Mol. Biol. *425*, 2878–2893.

Bougarne, N., Weyers, B., Desmet, S.J., Deckers, J., Ray, D.W., Staels, B., and De Bosscher, K. (2018). Molecular actions of PPARα in lipid metabolism and inflammation. Endocr. Rev. *39*, 760–802.

Bruning, J.B., Chalmers, M.J., Prasad, S., Busby, S.A., Kamenecka, T.M., He, Y., Nettles, K.W., and Griffin, P.R. (2007). Partial agonists activate PPARgamma using a helix 12 independent mechanism. Structure *15*, 1258–1271.

Brust, R., Shang, J., Fuhrmann, J., Mosure, S.A., Bass, J., Cano, A., Heidari, Z., Chrisman, I.M., Nemetchek, M.D., Blayo, A.L., et al. (2018). A structural mechanism for directing corepressor-selective inverse agonism of PPARgamma. Nat. Commun. *9*, 4687.

Capelli, D., Cerchia, C., Montanari, R., Loiodice, F., Tortorella, P., Laghezza, A., Cervoni, L., Pochetti, G., and Lavecchia, A. (2016). Structural basis for PPAR partial or full activation revealed by a novel ligand binding mode. Sci. Rep. *6*, 34792.

Chamoto, K., Chowdhury, P.S., Kumar, A., Sonomura, K., Matsuda, F., Fagarasan, S., and Honjo, T. (2017). Mitochondrial activation chemicals synergize with surface receptor PD-1 blockade for T cell-dependent antitumor activity. Proc. Natl. Acad. Sci. U S A *114*, E761–E770.

Da'adoosh, B., Marcus, D., Rayan, A., King, F., Che, J., and Goldblum, A. (2019). Discovering highly selective and diverse PPAR-delta agonists by ligand based machine learning and structural modeling. Sci. Rep. *9*, 1106.

Franssen, R., Vergeer, M., Stroes, E.S., and Kastelein, J.J. (2009). Combination statin-fibrate therapy: safety aspects. Diabetes Obes. Metab. *11*, 89–94.

Fyffe, S.A., Alphey, M.S., Buetow, L., Smith, T.K., Ferguson, M.A., Sørensen, M.D., Björkling, F., and Hunter, W.N. (2006). Recombinant human

PPAR-beta/delta ligand-binding domain is locked in an activated conformation by endogenous fatty acids. J. Mol. Biol. *356*, 1005–1013.

Graham, D.J., Staffa, J.A., Shatin, D., Andrade, S.E., Schech, S.D., La Grenade, L., Gurwitz, J.H., Chan, K.A., Goodman, M.J., and Platt, R. (2004). Incidence of hospitalized rhabdomyolysis in patients treated with lipid-lowering drugs. JAMA *292*, 2585–2590.

Han, L., Shen, W.J., Bittner, S., Kraemer, F.B., and Azhar, S. (2017). PPARs: regulators of metabolism and as therapeutic targets in cardiovascular disease. Part I: PPAR-alpha. Future Cardiol. *13*, 259–278.

Hassell, A.M., An, G., Bledsoe, R.K., Bynum, J.M., Carter, H.L., 3rd, Deng, S.J., Gampe, R.T., Grisard, T.E., Madauss, K.P., Nolte, R.T., et al. (2007). Crystallization of protein-ligand complexes. Acta Crystallogr. D Biol. Crystallogr. *63*, 72–79.

Ido, A., Hiromori, Y., Meng, L., Usuda, H., Nagase, H., Yang, M., Hu, J., and Nakanishi, T. (2017). Occurrence of fibrates and their metabolites in source and drinking water in Shanghai and Zhejiang, China. Sci. Rep. *7*, 45931.

Itoh, T., Fairall, L., Amin, K., Inaba, Y., Szanto, A., Balint, B.L., Nagy, L., Yamamoto, K., and Schwabe, J.W. (2008). Structural basis for the activation of PPARγ by oxidized fatty acids. Nat. Struct. Mol. Biol. *15*, 924–931.

Kamata, S., Yamamoto, J., Ohtani, H., Tosaka, Y., Yoshikawa, S., Akahoshi, N., and Ishii, I. (2018). 2D DIGE proteomic analysis reveals fasting-induced protein remodeling through organ-specific transcriptional factor(s) in mice. FEBS Open Bio *8*, 1524–1543.

Kawasaki, M., Kambe, A., Yamamoto, Y., Arulmozhiraja, S., Ito, S., Nakagawa, Y., Tokiwa, H., Nakano, S., and Shimano, H. (2020). Elucidation of molecular mechanism of a selective PPARalpha modulator, pemafibrate, through combinational approaches of X-ray crystallography, Thermodynamic analysis, and first-principle calculations. Int. J. Mol. Sci. *21*, 361.

Kojetin, D.J., and Burris, T.P. (2013). Small molecule modulation of nuclear receptor conformation dynamics: implication for functin and drug discovery. Mol. Pharm. *83*, 1–8.

Kuwabara, N., Oyama, T., Tomioka, D., Ohashi, M., Yanagisawa, J., Shimizu, T., and Miyachi, H. (2012). Peroxisome proliferator-activated receptors (PPARs) have multiple binding points that accommodate ligands in various conformations: phenylpropanoic acid-type PPAR ligands bind to PPAR in different conformations, depending on the subtype. J. Med. Chem. *55*, 893–902.

Leesnitzer, L.M., Parks, D.J., Bledsoe, R.K., Cobb, J.E., Collins, J.L., Consler, T.G., Davis, R.G., Hull-Ryde, E.A., Lenhard, J.M., Patel, L., et al. (2002). Functional consequences of cysteine modification in the ligand binding sites of peroxisome proliferator activated receptors by GW9662. Biochemistry *41*, 6640–6650.

Nolte, R.T., Wisely, G.B., Westin, S., Cobb, J.E., Lambert, M.H., Kurokawa, R., Rosenfeld, M.G., Willson, T.M., Glass, C.K., and Milburn, M.V. (1998). Ligand binding and co-activator assembly of the peroxisome proliferator-activated receptor-gamma. Nature *395*, 137–143.

Oyama, T., Toyota, K., Waku, T., Hirakawa, Y., Nagasawa, N., Kasuga, J.I., Hashimoto, Y., Miyachi, H., and Morikawa, K. (2009). Adaptability and selectivity of human peroxisome proliferator-activated receptor (PPAR) pan agonists revealed from crystal structures. Acta Crystallogr. D Biol. Crystallogr. *65*, 786–795.

Rakhshandehroo, M., Knoch, B., Muller, M., and Kersten, S. (2010). Peroxisome proliferator-activated receptor alpha target genes. PPAR Res. *2010*, 612089.

Shang, J., Brust, R., Mosure, S.A., Bass, J., Munoz-Tello, P., Lin, H., Hughes, T.S., Tang, M., Ge, Q., Kamenekca, T.M., et al. (2018). Cooperative cobinding of synthetic and natural ligands to the nuclear receptor PPARgamma. Elife *7*, e43320.

WHO. (2017). Cardiovascular Dieseases. https://www.who.int/news-room/fact-sheets/detail/cardiovascular-diseases-(cvds).

Wu, C.C., Baiga, T.J., Downes, M., La Clair, J.J., Atkins, A.R., Richard, S.B., Fan, W., Stockley-Noel, T.A., Bowman, M.E., Noel, J.P., et al. (2017). Structural basis for specific ligation of the peroxisome proliferator-activated receptor delta. Proc. Natl. Acad. Sci. U S A *114*, E2563–E2570.

Xu, H.E., Lambert, M.H., Montana, V.G., Parks, D.J., Blanchard, S.G., Brown, P.J., Sternbach, D.D., Lehmann, J.M., Wisely, G.B., Willson, T.M., et al. (1999). Molecular recognition of fatty acids by peroxisome proliferator-activated receptors. Mol. Cell *3*, 397–403.

Xu, H.E., Lambert, M.H., Montana, V.G., Plunket, K.D., Moore, L.B., Collins, J.L., Oplinger, J.A., Kliewer, S.A., Gampe, R.T., Jr., McKee, D.D., et al. (2001). Structural determinants of ligand binding selectivity between the peroxisome proliferator-activated receptors. Proc. Natl. Acad. Sci. U S A *98*, 13919–13924.

Xu, H.E., Stanley, T.B., Montana, V.G., Lambert, M.H., Shearer, B.G., Cobb, J.E., McKee, D.D., Galardi, C.M., Plunket, K.D., Nolte, R.T., et al. (2002). Structural basis for antagonist-mediated recruitment of nuclear co-repressors by PPARalpha. Nature *415*, 813–817.

Yamashita, S., Masuda, D., and Matsuzawa, Y. (2019). Clinical applications of a novel selective PPARalpha modulator, pemafibrate, in dyslipidemia and metabolic diseases. J. Atheroscler. Thromb. *26*, 389–402.

Yamashita, S., Masuda, D., and Matsuzawa, Y. (2020). Pemafibrate, a new selective PPARα modulator: drug concept and its clinical applications for dyslipidemia and metabolic diseases. Curr. Atheroscler. Rep. *22*, 5.

Yokote, K., Yamashita, S., Arai, H., Araki, E., Suganami, H., and Ishibashi, S.; Of The K-Study Group OB. (2019). Long-term efficacy and safety of pemafibrate, a novel selective peroxisome proliferator-activated receptor-alpha modulator (SPPARMalpha), in dyslipidemic patients with renal impairment. Int. J. Mol. Sci. *20*, 706.

Zoete, V., Grosdidier, A., and Michielin, O. (2007). Peroxisome proliferator-activated receptor structures: ligand specificity, molecular switch and interactions with regulators. Biochim. Biophys. Acta *1771*, 915–925.

iScience, Volume *23*

Supplemental Information

PPARα Ligand-Binding Domain Structures with Endogenous Fatty Acids and Fibrates

Shotaro Kamata, Takuji Oyama, Kenta Saito, Akihiro Honda, Yume Yamamoto, Keisuke Suda, Ryo Ishikawa, Toshimasa Itoh, Yasuo Watanabe, Takahiro Shibata, Koji Uchida, Makoto Suematsu, and Isao Ishii

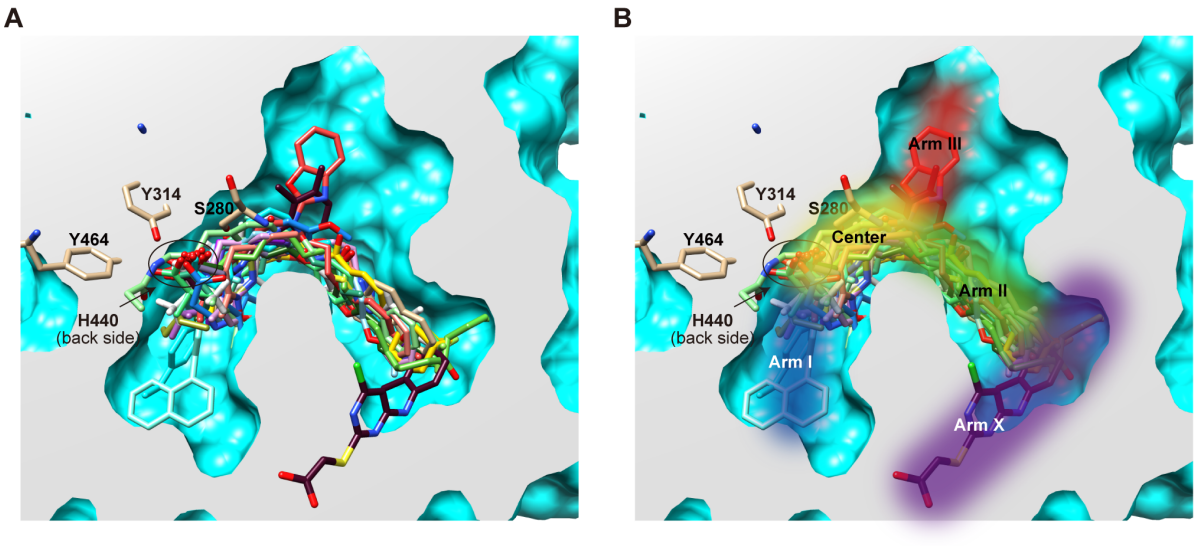

Figure S1. Twenty-one PPARα ligands located in PPARα-LBD, Related to Figures 1–4

(A) Twenty-one PPARα ligands, including 20 agonists and 1 antagonist, located in PPARα-LBD in the PDB registered crystal structures. (B) Five regions of PPARα-LBD (Arm I–III and X, and Center). A binding site for carboxylic residues common to PPARα ligands (*circled*) is surrounded by four amino acids (S280, Y314, H440, and Y464) and located between Arm I and Center regions. Pemafibrate is located deep in Arm III with its benzoxazole ring (*red*) (Kawasaki *et al.*, 2020), and one of the two Wy14643 molecules is found to be located in Arm X (Bernardes *et al.*, 2013). Only two ligands, 2-methyl-2-[4-(naphthalen-1-yl)phenoxy]propanoic acid and (2S,3S)-1-(4-methoxyphenyl)-3-(3-(2-(5-methyl-2-phenyloxazol-4-yl)ethoxy)benzyl)-4-oxoazetidine-2-carboxyl ic acid (65W and REW, respectively, in Table S1), are located in Arm I.

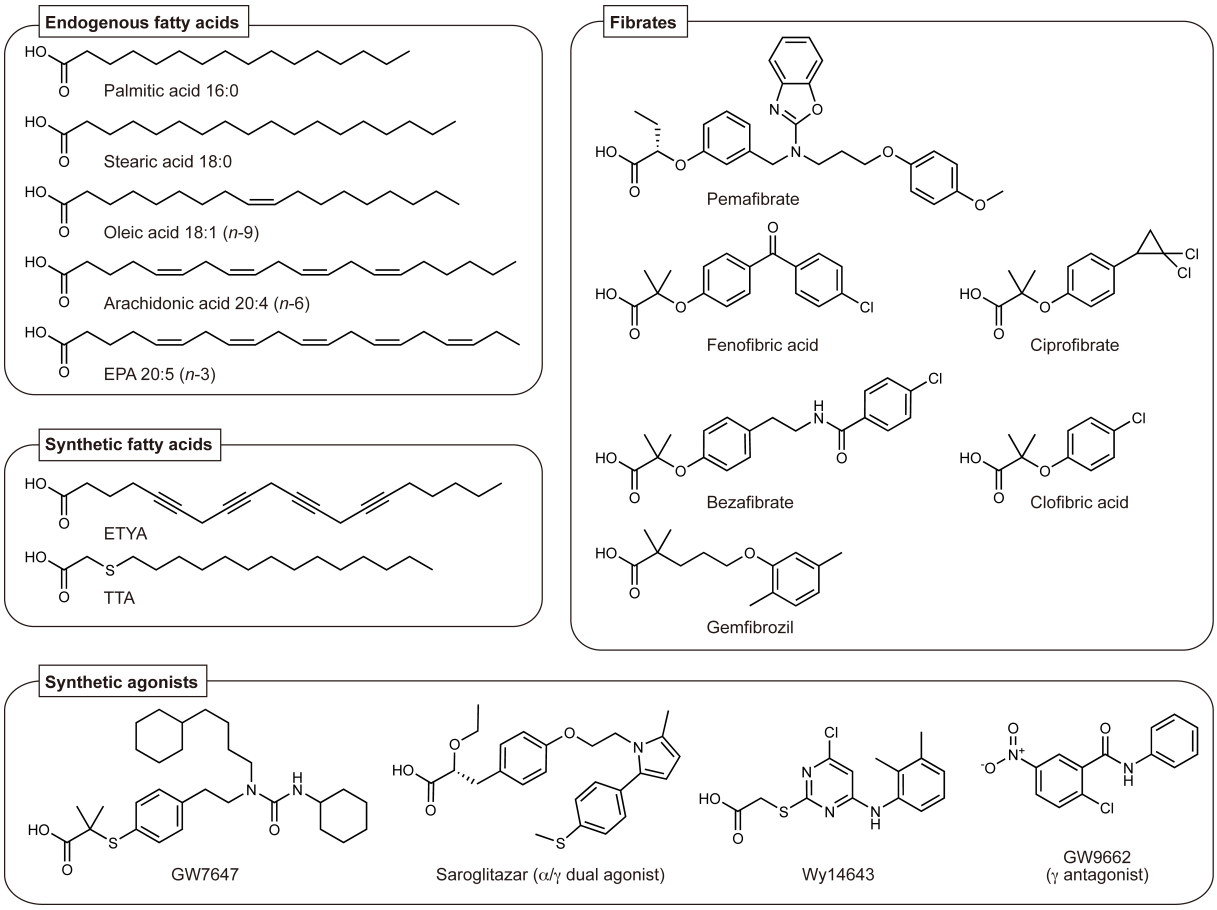

Figure S2. Chemical structures of 17 PPARα ligands analyzed in this study, Related to Figure 1
Five endogenous fatty acids, including EPA, two synthetic fatty acids (ETYA, 5,8,11,14-eicosatetraynoic acid [arachidonic acid mimetic]; TTA, tetradecylthioacetic acid, which is a PPAR pan agonist), six clinically approved fibrates, and four synthetic agonists, including saroglitazar, which is a PPARα/γ dual agonist, and GW9662, which is a PPARγ-selective antagonist.

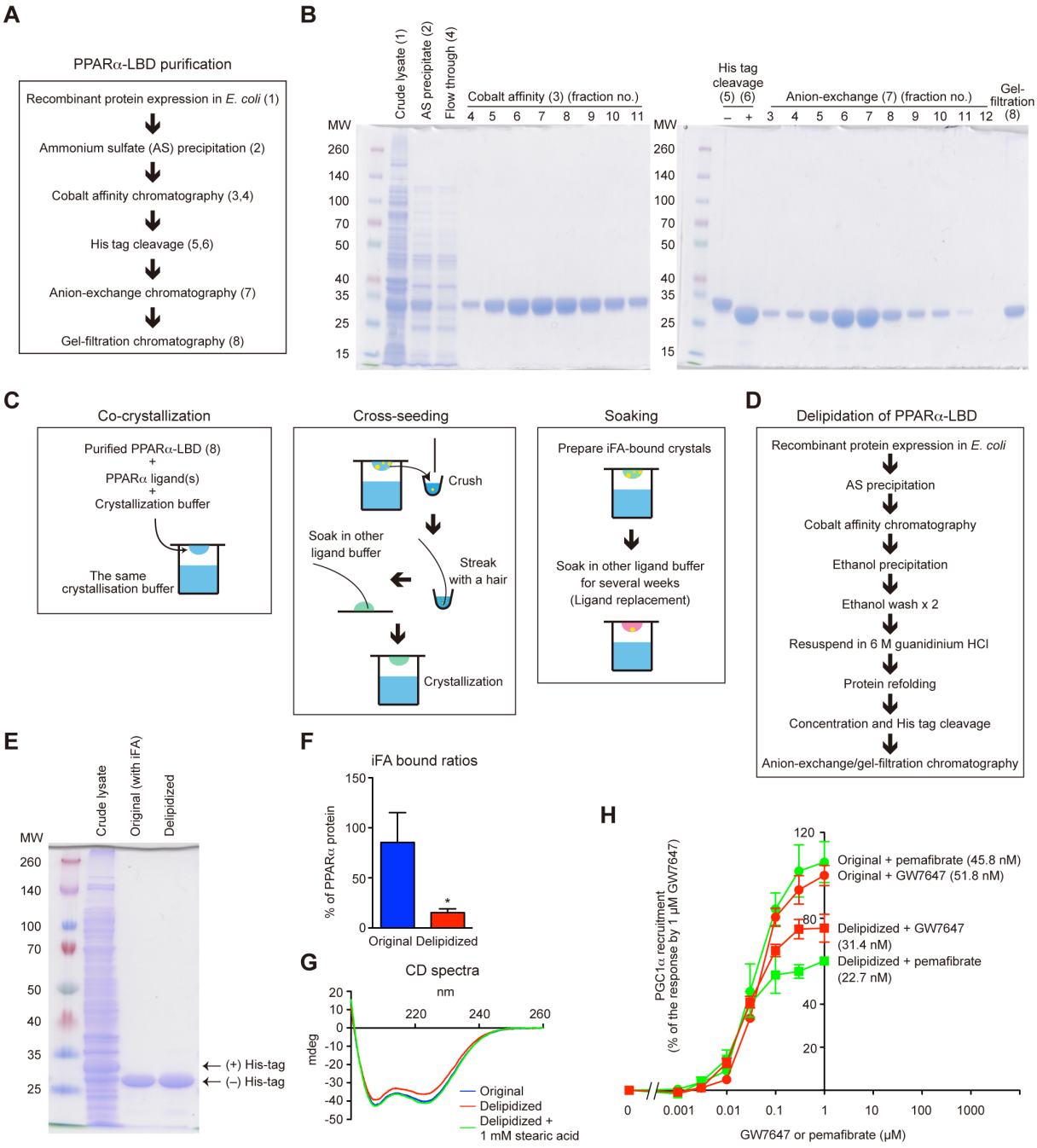

Figure S3. Methods for purification, delipidation, and crystallization of human PPARα-LBD proteins, and a functional assay of delipidized proteins, Related to Figure 1

(A, B) Methods (A) and SDS-PAGE gel check (B) of three-step chromatography for PPARα-LBD purification. (C) The different crystal preparation methods used in this study: co-crystallization, cross-seeding, and soaking. (D) Delipidation procedures to remove intrinsic fatty acid (iFA). (E) SDS-PAGE gel check of delipidized PPARα-LBD. (F–H) Comparative analyses of original and delipidized PPARα-LBD using iFA-bound ratios (F), circular dichroism (CD) spectra (G), PPARα activation (PGC1α recruitment) by agonists (H). The difference is significant ($^{*}P<0.05$) in (F). Stearic acid supplementation (1 mM) restored the CD spectrum shift by delipidation in (G). Similar EC_{50} values (in parentheses) were obtained from pemafibrate/GW7647 concentration-dependent activation of original (iFA-bound) and delipidized PPARα-LBD proteins.

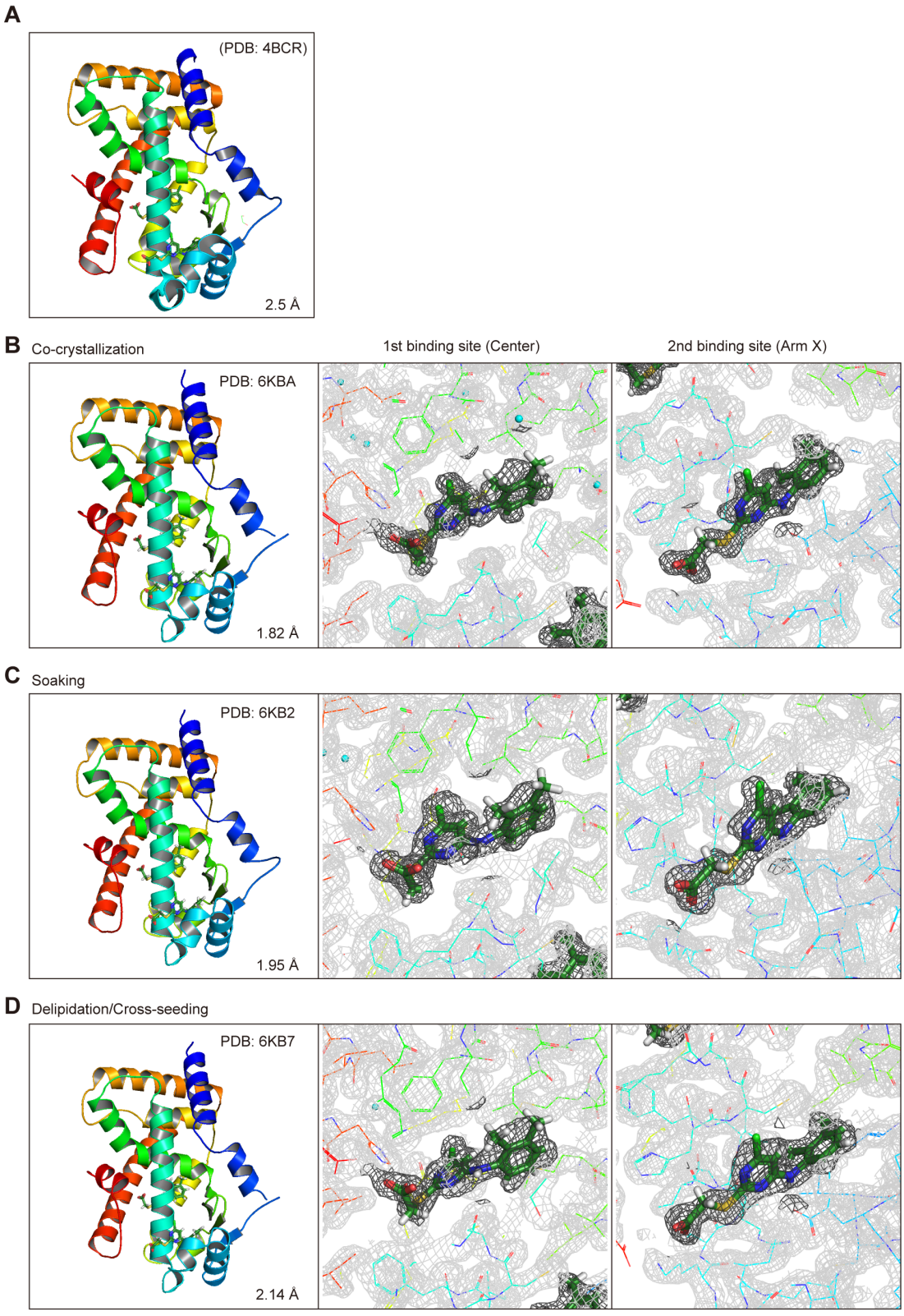

Figure S4. Crystal structures of PPARα-LBD bound to two Wy14643 molecules by different crystal preparation methods, Related to Figure 1

(A) PDB (ID: 4BCR): Deposited Wy14643 (×2)-bound structure deposited (Bernardes *et al.*, 2013). (B–D) Overall structures and magnified views of two Wy14643 binding sites, located in the Center and Arm X regions, in crystals obtained using co-crystallization (B), soaking (C), or delipidation/cross-seeding (D) procedures. The electron density is shown in the mesh using Feature Enhanced Maps (FEMs) contoured at 1.0σ. PDB identities and resolutions are labelled, and water molecules are presented as cyan spheres.

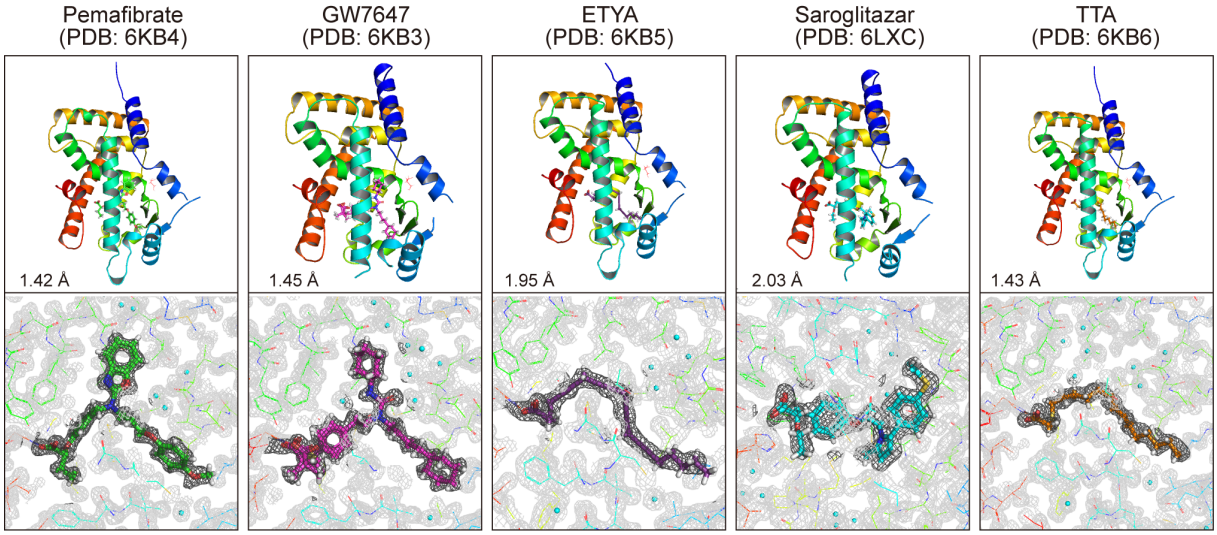

Figure S5. Crystal structures and magnified views of PPARα-LBD and five potent PPARα agonists obtained using cross-seeding of the delipidized proteins, Related to Figure 2

The electron density is shown in the mesh by FEMs contoured at 1.0σ. PDB identities and resolutions are labelled, and water molecules are presented as cyan spheres.

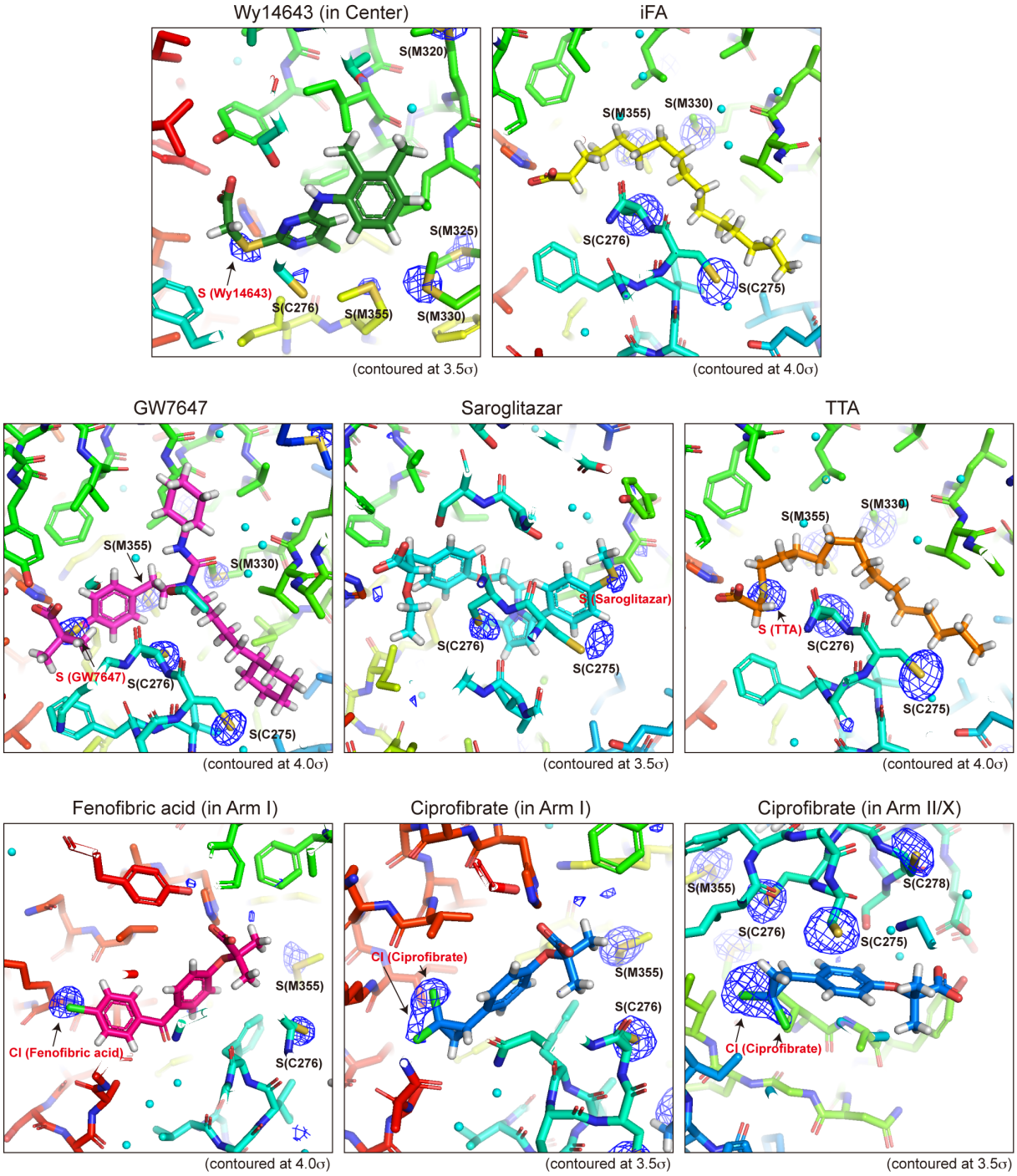

Figure S6. Magnified views of PPARα-LBD–ligand structures superimposed with sulfur/chloride signals located using anomalous difference Fourier maps, Related to Figure 2

PPARα agonists, such as Wy14643, GW7647, saroglitazar, and TTA, but not intrinsic fatty acid, have been found to possess single sulfur atoms in their molecules, which are detectable using anomalous difference Fourier maps, contoured at 3.5σ or 4.0σ, conducted with 1.8 Å X-ray. Chloride signals in fenofibric acid and ciprofibrate were also detected. The electron density is shown in the mesh, and water molecules are presented as cyan spheres. The locations of all the sulfur/chloride signals correspond to the signals revealed by routine 1.0 Å X-ray crystallography.

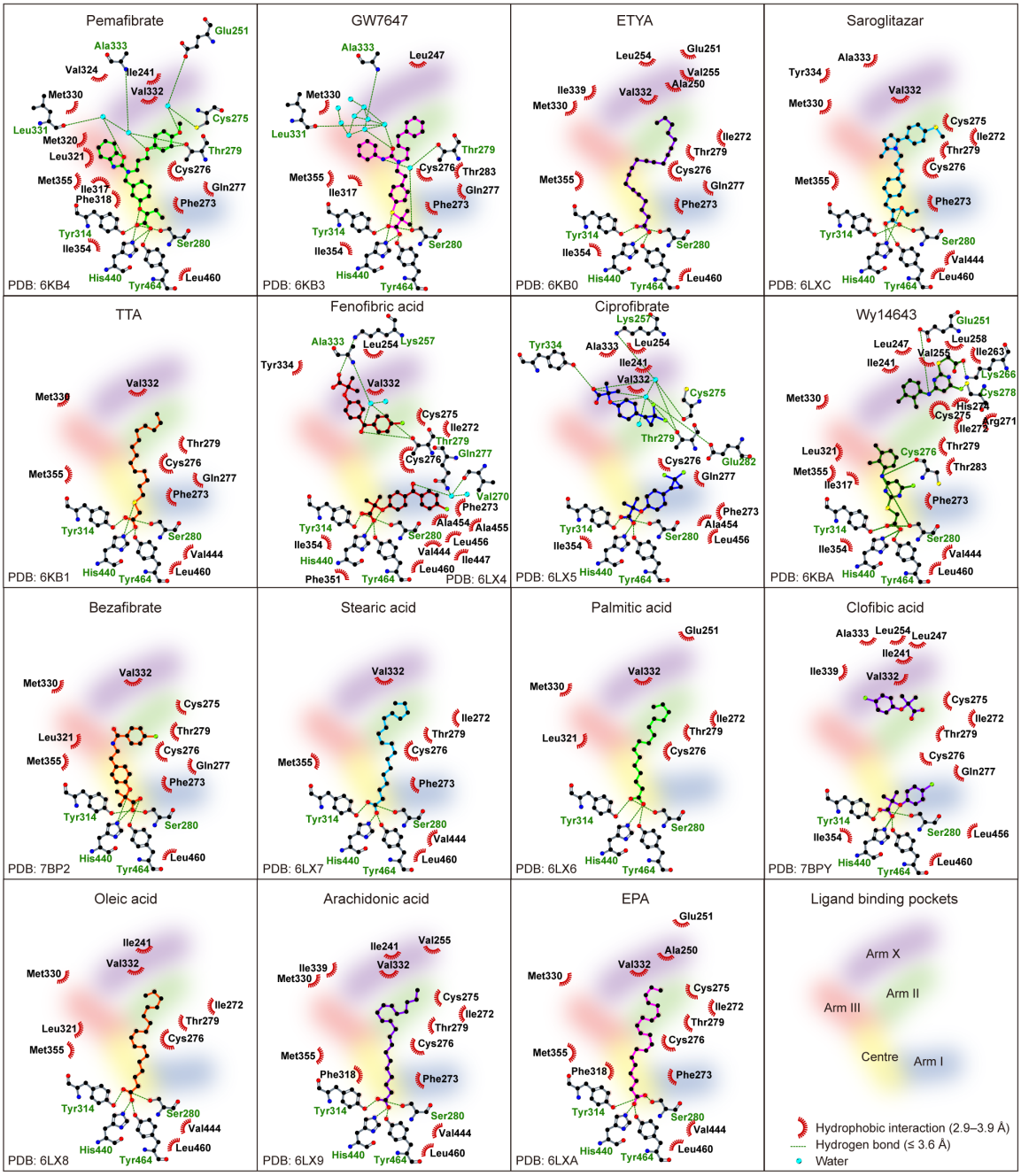

Figure S7. Interatomic interaction of 15 ligands with PPARα-LBDs, Related to Figures 2 and 3
Conserved hydrogen bonds, including those between the carboxyl groups of ligands and their surrounding S280, Y314, H440, and Y464 residues in Arm I/Center boundary, are illustrated by green dashed lines. All plots were generated using LigPlot+.

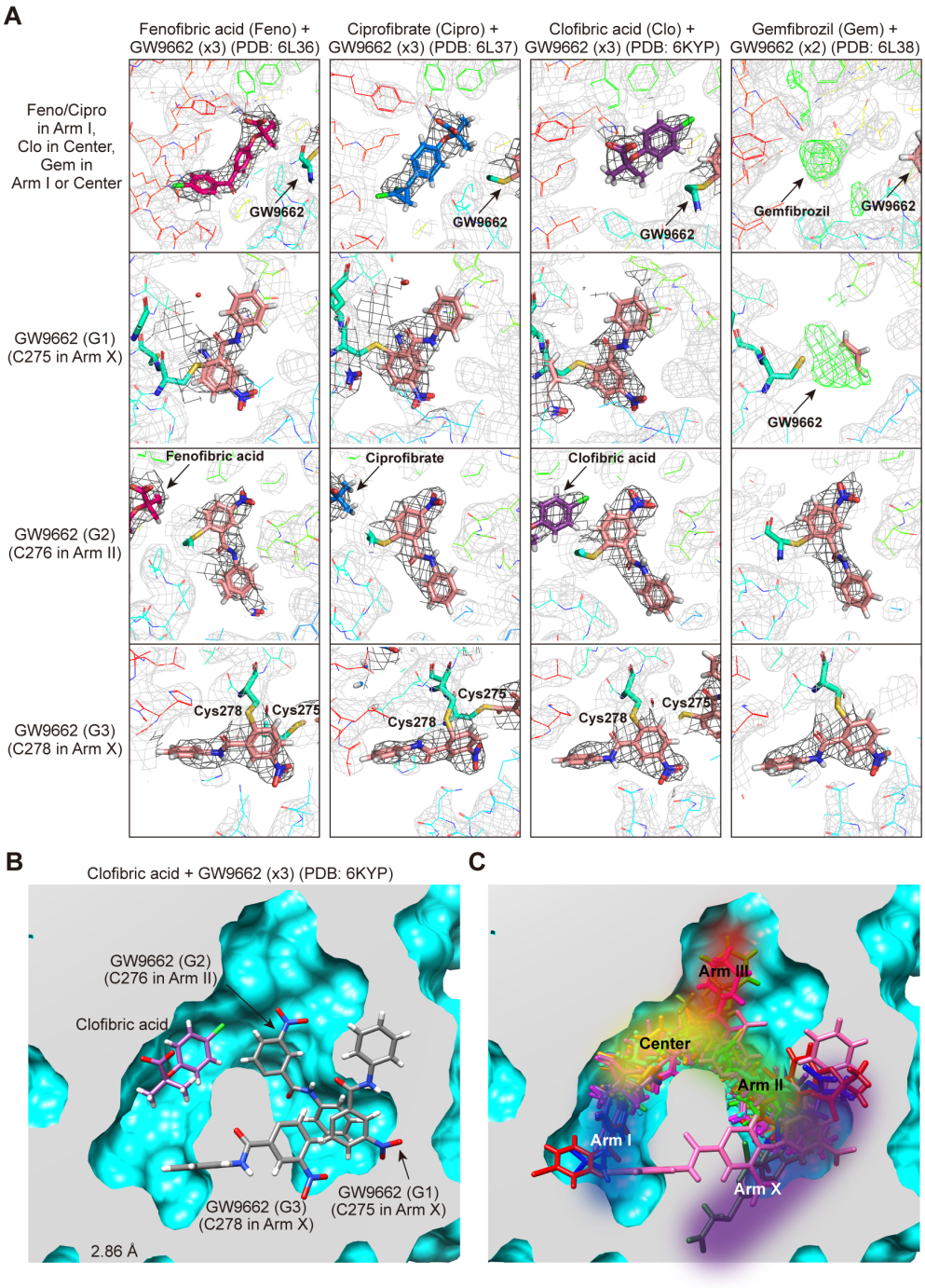

Figure S8. Magnified views of crystal structures of PPARα-LBD with fibrates and GW9662 and enlarged LBD spaces by this study, Related to Figure 4

(A) Fenofibric acid and ciprofibrate are located at Arm I (two sites, Arm I and II/X boundary, in the absence of GW9662), whereas three GW9662 are located at Arm II and X; one molecule is covalently bound to Cys276 in Arm II, and two molecules are covalently bound to Cys275 and Cys278 in Arm X. Clofibric acid is located at the Center or at Arm I in the absence of GW9662, and three GW9662 are located similarly. Although no crystals were obtained with gemfibrozil alone, crystals with combinations of gemfibrozil and GW9662 were acquired. Only unclear electron densities of gemfibrozil, in the Center, and single GW9662 molecule, attached to Cys275, were obtained, but two GW9662 were covalently bound to Cys276 in Arm II and Cys275 in Arm X, explicitly. The electron density is shown in the black mesh using FEMs contoured at 1.0σ and in the green mesh, only for gemfibrozil crystals, using *F*o-*F*c omit maps contoured at 3.0σ. (B) A magnified view of PPARα-LBD bound with clofibric acid/GW9662 (×3). (C) Enlarged PPARα-LBD spaces from the results of this study. Original spaces for four Arms and Center regions (the same in Figure S1B) are illustrated.

Table S1. Twenty-one PPARα-LBD X-ray crystal structures deposited so far in the Protein Data Bank (PDB) to date, Related to Table 1

PDB ID	Resolution	Ligand(s)	Publication	Released date
3VI8	1.75 Å	13M	*J. Med. Chem.* 55, 893–902 (2012)	2012/8/29
2P54	1.79 Å	735	*J. Med. Chem.* 50, 685–695 (2007)	2007/4/24
5HYK	1.83 Å	65W	*Sci. Rep.* 6, 34792 (2016)	2016/11/23
6KXX	1.95 Å	T02	*Sci. Rep.* 10, 4623 (2020)	2020/5/20
6KXY	2.00 Å	T06	*Sci. Rep.* 10, 4623 (2020)	2020/5/20
2ZNN	2.01 Å	S44	*Acta Crystallogr. D Biol. Crystallogr.* 65, 786–795 (2009)	2009/5/5
3KDU	2.07 Å	NKS	*J. Med. Chem.* 53, 2854–2864 (2010)	2010/4/28
1I7G	2.2 Å	AZ2	*Structure* 9, 699–706 (2001)	2002/3/9
3G8I	2.2 Å	RO7	*Bioorg. Med. Chem. Lett.* 19, 2468–2473 (2009)	2009/6/2
3SP6	2.21 Å	IL2	*J. Biol. Chem.* 286, 31473–31479 (2011)	2011/7/20
2NPA	2.3 Å	MMB	*Bioorg. Med. Chem. Lett.* 17, 937–941 (2007)	2007/10/30
4Cl4	2.3 Å	Y1N	*J. Struct. Biol.* 191, 332–340 (2015)	2014/12/24
2REW	2.35 Å	REW	Not published	2007/11/27
3FEI	2.4 Å	CTM	*ChemMedChem* 4, 951–956 (2009)	2009/10/20
1K7L	2.5 Å	544	*Proc. Natl. Acad. Sci. USA* 98, 13919–13924 (2001)	2001/12/5
3ET1	2.5 Å	ET1	*Proc. Natl. Acad. Sci. USA* 106, 262–267 (2009)	2009/2/17
4BCR	2.5 Å	WY1	*J. Mol. Biol.* 425, 2878 (2013)	2013/5/29
3KDT	2.7 Å	7HA	*J. Med. Chem.* 53, 2854–2864 (2010)	2010/4/28
1KKQ	3.0 Å	471	*Nature* 415, 813–817 (2002)	2002/2/20
6L96	3.20 Å	P7F	*Int. J. Mol. Sci.* 21, 361 (2020)	2020/1/6
5AZT	3.45 Å	4M5	*ACS Chem.Biol.* 11, 2447–2455 (2016)	2016/7/6

Data are ordered by the highest resolutions of crystal structures.

TRANSPARENT METHODS

Key Resources Table

REAGENT or RESOURCE	SOURCE	IDENTIFIER
Antibodies		
Eu-W1024-labelled anti-6×His antibody	PerkinElmer	Cat#AD0205; RRID: AB_2811261
Bacterial and Virus Strains		
Escherichia coli Rosetta (DE3) pLysS	Novagen	Cat#70956
Biological Samples		
Human blood	This paper	N/A
Chemicals, Peptides, and Recombinant Proteins		
Polyethyleneimine	Fujifilm-Wako	Cat#167-11951; CAS: 9002-98-6
d_{33}-Oleic acid	Cambridge Isotope Laboratories	Cat#DLM-1891-PK
Polyethylene glycol (PEG) 3,350	Hampton Research	Cat#HR2-144; CAS: 25322-68-3
SRC1 pentadecenoyl peptide (LTERHKILHRLLQEG)	GenScript	N/A
GW7647	Cayman Chemical	Cat#10008613; CAS: 265129-71-3
Bezafibrate	Cayman Chemical	Cat#10009145; CAS: 41859-67-0
Tetradecylthioacetic Acid	Fujifilm-Wako	Cat#209-18141; CAS: 2921-20-2
Wy14643	Cayman Chemical	Cat#70730; CAS: 50892-23-4
GW9662	Cayman Chemical	Cat#70785; CAS: 22978-25-2
Ciprofibrate	Fujifilm-Wako	Cat#033-21191; CAS: 52214-84-3
Fenofibric acid	Combi-Blocks	Cat#OR-1173; CAS: 42017-89-0
5, 8, 11, 14-Icosatetraynoic Acid	Cayman Chemical	Cat#90120; CAS: 1191-85-1
Icosapentaenoic Acid	Cayman Chemical	Cat#90110; CAS: 10417-94-4
Clofibric Acid	LKT Labs	Cat#C4556; CAS: 882-09-7
Gemfibrozil	Combi-Blocks	Cat#OR-0524; CAS: 25812-30-0
Arachidonic acid	Cayman Chemical	Cat#10006607; CAS: 6610-25-9
Pemafibrate	Chemscene	Cat# CS-6084; CAS: 848259-27-8
Saroglitazar	Chemscene	Cat# CS-6149; CAS: 495399-09-2
Myristic acid	Nacalai Tesque	Cat#23517-82; CAS: 544-63-8
Palmitic acid	Sigma-Aldrich	Cat#P0500-10G; CAS: 57-10-3
Stearic acid	Sigma-Aldrich	Cat#S4751-1G; CAS: 57-11-4
Oleic acid	Nacalai Tesque	Cat#25630-51; CAS: 112-80-1
Linoleic acid	Nacalai Tesque	Cat#20513-41; CAS: 60-33-3
α-Linolenic acid	Cayman Chemical	Cat#90210; CAS: 463-40-1
Vaccenic Acid	Sigma-Aldrich	Cat#V1131-100MG; CAS: 693-72-1

Biotin-labelled PGC1α peptides (biotin-EAEEPSLLKKLLLAPANTQ	GenScript	N/A
ULight-Streptavidin	PerkinElmer	Cat#TRF0102
Critical Commercial Assays		
NEFA C-test Wako	Fujifilm-Wako	Cat#279-75401
AMP+ mass spectrometry kit	Cayman Chemical	Cat#710000
Crystal Screen	Hampton Research	Cat#HR2-110
Crystal Screen 2	Hampton Research	Cat#HR2-112
Index	Hampton Research	Cat#HR2-144
PrimeSTAR mutagenesis basal kit	Takara Bio	Cat#R046A
Deposited Data		
34 novel hPPARα-LBD structures in this study	Protein Data Bank (PDB)	Table 1
21 hPPARα-LBD structures so far deposited in PDB	Protein Data Bank (PDB)	Table S1
Recombinant DNA		
pET28a encoding human PPARα residues 200–468	Oyama et al., 2009	N/A
Software and Algorithms		
XDS v-Jan 26 2018 or Mar 15 2019	Kabsch, 2010	http://xds.mpimf-heidelberg.mpg.de/; RRID: SCR_015652
Aimless v-0.5.21	Evans & Murshudov, 2013	https://www.ccp4.ac.uk/; RRID: SCR_015747
Phaser v-2.7.6	McCoy et al., 2007	https://www.ccp4.ac.uk/; RRID: SCR_014219
Phenix v-1.11.1-2575-000	Adams et al., 2010	https://www.phenix-online.org/; RRID: SCR_014224
Coot v-0.8.2	Emsley & Cowtan, 2004	https://www.ccp4.ac.uk/; RRID: SCR_014222
PyMOL v-1.8.x	Schrodinger	https://pymol.org/2/; RRID: SCR_000305
UCSF Chimera v-1.10.2	Pettersen et al., 2004	https://www.cgl.ucsf.edu/chimera/; RRID: SCR_004097
LigPlot+ v-1.4.5	Laskowski & Swindells, 2011	https://www.ebi.ac.uk/thornton-srv/software/LigPlus/; RRID: SCR_018249
GraphPad Prism v-5.0c	GraphPad Software	https://www.graphpad.com/scientific-software/prism/; RRID: SCR_002798
Other		
TALON Metal Affinity Resin	Clontech	Cat#635682
HiTrap Q	GE Healthcare	Cat#17115301
HiLoad 16/600 Superdex 75 pg gel-filtration column	GE Healthcare	Cat#28989333
Slide-A-Lyzer G2 Dialysis Cassette	Thermo Fisher	Cat#87735
Develosil HB-C30-UG 3 μm column, 100 × 2.0 mm	Nomura Chemical	Cat#HBUG173201001

PPARα-LBD expression and purification

Human PPARα-LBD (amino acids 200–468) was expressed as an amino-terminal His-tagged protein from a pET28a vector (Novagen) in Rosetta (DE3) pLysS competent cells (Novagen) and was purified by three-step chromatography (Capelli *et al.*, 2016; Oyama *et al.*, 2009) with some modifications. Transformed cells were cultured in LB medium (with 15 μg/ml kanamycin and 34 μg/ml chloramphenicol) at 30 °C, and 50 mL of overnight culture was seeded in 1 L of TB medium (with 15 μg/ml kanamycin), which was cultured at 30 °C for 1.5 h and then at 15 °C for 2 h. Protein overexpression was induced by adding 0.5 mM isopropyl β-D-galactopyranoside, which was later cultured at 15 °C for 48 h. The cells were harvested and resuspended in 40

mL buffer A (20 mM Tris-HCl (pH 8.0), 150 mM NaCl, 1 mM Tris 2-carboxyethylphosphine (TCEP)-HCl, and 10% glycerol) containing a cOmplete EDTA-free protease inhibitor (Sigma-Aldrich). The cells were then lysed by sonication for 2 min five times at an output of 8 with a UD-201 sonicator (Tomy, Tokyo, Japan) and clarified using centrifugation at 12,000 *g*, for 20 min, at 4 °C (the same conditions were used subsequently unless otherwise noted), and polyethyleneimine was added with a final concentration of 0.15% (v/v) to the supernatant in order to remove nucleic acids. After centrifugation, 35 ml of the supernatant was mixed with 20 g of ammonium sulfate at 4 °C for 30 min using gentle rotation. After centrifugation, the pellet was resuspended in 30 mL of buffer B, which was buffer A plus 10 mM imidazole. The suspension was loaded on a cobalt-based immobilized metal affinity column (TALON Metal Affinity Resin, Clontech), equilibrated with buffer B, and eluted with a linear gradient of 10–100 mM imidazole. The PPARα-LBD-containing elutes (e.g., fraction nos. 5–10 in Figure S3B, left) were incubated with 33 U/ml thrombin protease (Nacalai Tesque, Kyoto, Japan) to cleave His tag and, at the same time, dialyzed against buffer A overnight at 4 °C using a Slide-A-Lyzer G2 Dialysis Cassette (20-kDa cutoff, Thermo Fisher Scientific). Then, the sample was later dialyzed against buffer C, which was buffer A minus 150 mM NaCl, at 4 °C for 3 h. The sample was then loaded onto a HiTrap Q anion-exchange column (GE Healthcare), equilibrated with buffer C, and eluted with a linear gradient of 0–150 mM NaCl. The elutes (e.g., fraction nos. 6–7 in Figure S3B, right) were loaded onto a HiLoad 16/600 Superdex 75 pg gel-filtration column (GE Healthcare), equilibrated with buffer A, and eluted with buffer A. The purity of human PPARα-LBD was continuously analyzed using SDS-PAGE and Coomassie Brilliant Blue staining (Figure S3B).

Measurement of fatty acid contents in PPARα-LBD and human serum

The total free fatty acid levels in PPARα-LBD proteins were measured using the NEFA C-test Wako for *in vitro* diagnosis (Fujifilm-Wako, Osaka, Japan). To analyze their contents, a 10 µl aliquot of PPARα-LBD proteins (20 mg/ml) was transferred to a clean glass tube containing 100 pmol d33-oleic acid as an internal standard. Lipids were extracted using Bligh & Dyer methods (Bligh & Dyer, 1959). Then 30 µl of chloroform/methanol (1:2, v/v) was added and mixed well. Next, 10 µl of chloroform and then 10 µl of water were added to the samples, which were mixed well, and centrifuged at 3,000 *g*, for 5 min, at room temperature. Then, the lower organic phase was transferred to another glass tube and dried under a stream of argon gas. Free fatty acids were derivatized with *N*-(4-aminomethylphenyl)pyridinium (AMPP) using a AMP+ mass spectrometry kit (Cayman Chemical) as previously reported (Bollinger *et al.*, 2013). Briefly, the samples were resuspended in 5 µl ice-cold acetonitrile/dimethylformamide (4:1, v/v), and the following reagents were added: 5 µl of 640 mM 1-ethyl-3-(ε-dimethylaminopropyl)carbodiimide in water, 2.5 µl of 20 mM *N*-hydroxylbenzotriazole in acetonitrile/dimethylformamide 99:1, and 7.5 µl of 20 mM AMPP in acetonitrile. Then, the samples were mixed, incubated at 60 °C for 30 min, and analyzed on the same day.

The collection and lipid analyses of blood/serum were approved (no. 2019-5) by the Ethics Committee of Showa Pharmaceutical University with informed consent from all participants, and personal information was blinded to the experimenters. For the analysis of fatty acid contents in human serum, 8 µl aliquot of serum was transferred to a clean glass tube. Reagents were added to each tube: 2 µl of 4 mM d33-oleic acid, as an internal standard, 90 µl of water, 200 µl of chloroform, and 400 µl of methanol. The samples were mixed well. Then, 200 µl of chloroform and later 300 µl of water were added, mixed well, and centrifuged at 3,000 *g*, for 5 min, at room temperature. The lower organic phase was transferred to another glass tube and dried under a stream of argon gas.

Fatty acids in human plasma were also derivatized using the mass spectrometry kit. The samples were resuspended in 30 µl of ice-cold acetonitrile/dimethylformamide (4:1, v/v), and 20 µl of 640 mM 1-ethyl-3-(ε-dimethylamino-propyl)carbodiimide in water, 10 µl of 20 mM *N*-hydroxylbenzotriazole in acetonitrile/dimethylformamide 99:1, and 20 µl of 20 mM AMPP in acetonitrile were added. The samples were briefly mixed, incubated at 60 °C for 30 min, and analyzed on the same day.

Mass spectrometric analyses were performed using a Waters Xevo TQD triple quadrupole mass spectrometer interfaced to an ACQUITY ultra-performance liquid chromatography (UPLC) system (Waters). UPLC was carried out using a reverse-phase C30 column (Develosil HB-C30-UG 3-µm column, 100 × 2.0 mm, Nomura Chemical, Aichi, Japan). Solvent A was water containing 0.1% formic acid, and solvent B was acetonitrile containing 0.1% formic acid. The solvent program included linear gradients: 40% of solvent B at 0 min, 99% of solvent B at 8–10 min, and 40% of solvent B at 10.1 min. The flow rate was 0.3 ml/min, and the column temperature was set at 40 °C. Selected reaction monitoring (SRM) was performed in the positive ion mode using nitrogen as the nebulizing gas. The monitored SRM transitions were as follows: myristic acid, *m*/*z* 395.0 > 239.0; palmitic acid, *m*/*z* 423.0 > 239.0; stearic acid, *m*/*z* 451.0 > 239.0; oleic acid, *m*/*z* 449.0 > 239.0; linoleic acid, *m*/*z* 447.0 > 239.0; linolenic acid, *m*/*z* 445.0 > 239.0; arachidonic acid, *m*/*z* 471.0 > 239.0; and d33-oleic acid, *m*/*z* 482.6 > 242.3. The amounts of fatty acid derivatives were calculated using the ratios of the peak area of the target compounds and of the derivatized stable isotope (d33-oleic acid). MassLynx version 4.1 was used for the system control and data processing.

Delipidation of PPARα-LBD

The PPARα-LBD-containing elutes from the cobalt column were precipitated with 9× volumes of ethanol for 2 h at room temperature. After centrifugation at 15,000 *g* for 10 min at 4 °C, the pellet was washed twice using 90% ethanol, and resuspended in 20 mL of 6 M guanidinium hydrochloride in buffer A overnight at 4 °C. For refolding, the sample was directly diluted with 180 mL of buffer A and then concentrated by centrifugation to 3 mL using an Amicon Ultra-15 centrifugal filter (3-kDa cutoff, Merck Millipore). Thereafter, the sample was treated with thrombin and dialyzed with buffer A and was processed as described above.

Co-crystallization and soaking

After examining 192 different buffer conditions using the Crystal Screen and Crystal Screen 2, and Index crystallization kits from Hampton Research at 4 °C and 20 °C (Table S2), we were able to obtain characteristic rod-shaped Wy14643-bound crystals (Figure 1A) in 0.1 M Bis-Tris (pH 6.5)/25% (w/v) polyethylene glycol (PEG) 3,350 (no. 43 buffer in the Index kit) at 4 °C using co-crystallization, which gave a 1.82 Å resolution structure (Crystal no.15 in Table S3). Following this method, co-crystallization was performed in hanging-drop mixtures of 0.5 µl PPARα-LBD (20 mg/ml in buffer A), 0.5 µl ligand (200–2,000 µM in buffer A), and 1 µl reservoir solution (variations of no. 43 buffer: 0.1 M Bis-Tris (pH 6.5), 0.1 M HEPES (pH 7.0 or 7.5), or 0.1 M Tris (pH 8.0 or 8.5) with 25% PEG 3,350) at 4 °C for several weeks. To prepare the PPARα-LBD/ligand/coactivator crystals, 0.25 µl ligand (2 mM in buffer A) and 0.25 µl SRC1 pentadecenoyl peptide (LTERHKILHRLLQEG synthesized by GenScript) were used instead of the 0.5 µl ligand above. For the cross-seeding, Wy14643-bound crystals were crushed using small needles in the reservoir solution. Then, the crushed crystal powder was transferred to another PPARα-LBD/(another) ligand/reservoir solution using a single streak with a human crown

hair, and this was incubated at 4 °C for several weeks. For soaking, iFA-bound PPARα-LBD crystals were soaked in a reservoir solution (0.1 M HEPES (pH 7.5), 20% PEG 3,350) containing 0.5–5 mM ligand (final 0.1–1% DMSO) at 4 °C for several weeks. All crystals were briefly soaked in cryoprotection buffer (their respective reservoir solutions with 20% glycerol); afterwards, these were flash-cooled in a stream of liquid nitrogen until X-ray crystallography was conducted.

X-ray diffraction data collection and model refinement

Datasets were collected at four available beamlines (BL-5A, BL-17A, and AR-NE3A at the Photon Factory (Ibaraki, Japan) and BL26B1 at the SPring-8 (Hyogo, Japan)) using synchrotron radiation of 1.0 Å. X-ray diffraction data were also collected using 1.8 Å wavelength X-ray to identify sulfur and chloride atoms in some ligands by analyzing anomalous scattering signals included in X-ray diffraction data (Liu *et al.*, 2012). Although sulfur and chloride atoms have the absorption K-edge at wavelengths longer than 1.8 Å, the anomalous difference Fourier maps exhibited significant signals, which enabled to locate those atoms within the crystal structures. Diffraction data was collected at 0.1˚ oscillation per frame, and a total of 1,800 frames (180˚) were recorded for 1.0 Å X-ray crystallography and 3,600 (360˚) frames for 1.8 Å crystallography. Data processing and scaling were carried out using XDS X-ray detector software (Kabsch, 2010) and AIMLESS (Evans & Murshudov, 2013), respectively. Resolution cutoff values (R_{merge} < 0.5, R_{pim} < 0.3, and Completeness < 0.9) were set by the highest resolution shell. All structures were determined using molecular replacement in PHASER (McCoy *et al.*, 2007) and 1.75 Å resolution structures of synthetic ligand-containing human PPARα-LBD (PDB: 3VI8) (Table S1) as the starting model. Refinement of the structure was performed using iterative cycles of model adjustment in two programs: COOT (Emsley & Cowtan, 2004) and PHENIX (Adams *et al.*, 2010). All collection data and refinement statistics are included in Tables S3 and S4, and essential data are shown in Table 1 with web links to the PDB. *F*o-*F*c omit maps and Feature Enhanced Maps (FEMs) were calculated using PHENIX. The structures were constructed using PyMOL (http://www.pymol.org) and USCF Chimera (Pettersen *et al.*, 2004) programs. The interatomic interaction of ligands with PPARα-LBDs was investigated using LigPlot+ (Laskowski & Swindells, 2011).

PPARα activation (PGC1α coactivator recruitment) assay

Activation/inactivation status of PPARα can be determined using a time-resolved fluorescence resonance energy transfer (TR-FRET) assay, which is used for detecting physical interactions between His-tagged human PPARα-LBD proteins and biotin-labelled PGC1α coactivator peptides (biotin-EAEEPSLLKKLLLAPANTQ synthesized by GenScript) using a LANCE Ultra TR-FRET Assay (PerkinElmer). For the activation assay, 9.5 µl of PPARα-LBD (200 nM in buffer D (10 mM HEPES-HCl (pH7.4), 150 mM NaCl, 0.005% Tween 20, 0.1% fatty acid-free bovine serum albumin)), 0.5 µl of 100× ligand solution (in DMSO or ethanol), and 5 µl of biotin-PGC1α peptide (4 µM) were mixed in a single well of a Corning 384 well low volume white round bottom polystyrene non-binding surface microplate. Then, 5 µl of 4 nM Eu-W1024-labelled anti-6×His antibody (PerkinElmer)/80 nM ULight-Streptavidin (PerkinElmer) was added to each well and the microplate was incubated in the dark at room temperature for 2 h. FRET signals were detected at one excitation filter (340/12) and two emission filters (615/12 and 665/12) using the Varioskan Flash double monochromater microplate reader (Thermo Fisher Scientific). The parameters for the measurement at 615 nm and 665 nm were an integration time of 200 µs and a

delay time of 100 μs. The 665 nm emissions were due to ULight-FRET, and the 615 nm emissions were due to Eu-W1024. The 665/615 ratio was calculated and normalized to the negative control reaction using 1% DMSO. For the inactivation assay, graded concentrations of GW9662 were added in the presence of 1–3,000 μM of ligand. Nonlinear fitting and calculation of EC_{50} and IC_{50} were performed using Prism 5 software (GraphPad, San Diego, USA).

Thermostability assay using CD spectroscopy

Around 10 μM of the PPARα-LBD proteins was incubated with varied concentrations of ligands in buffer A. The CD spectra were monitored within 200–260 nm at increasing temperatures from 30 °C to 70 °C (2 °C/min) with the use of a J-1500 spectropolarimeter (JASCO, Tokyo, Japan), which is equipped with a PTC-510 thermal controller (JASCO). Approximate melting temperatures were obtained by fitting a single-site sigmoidal dose response curve using Prism 5.

Mutagenesis of PPARα-LBD cDNA

Site-directed mutagenesis (single amino acid substitutions) was performed using a PrimeSTAR Mutagenesis Basal Kit (Takara Bio). The Cys275Ser (C275S) and C276S but not C278S PPARα-LBD mutants displayed ligand-dependent activation (coactivator recruitment).

Quantification and Statistical Analysis

Data are presented as means ± SEM (*n*: numbers of independent experiments that have 3–4 well replicates) or means ± SD for the human samples. Statistical comparison was performed using an unpaired two-tailed Student's *t*-test in Prism 5. All *P*-values <0.05 denote a significant difference.

References

Adams, P.D., Afonine, P.V., Bunkóczi, G., Chen, V.B., Davis, I.W., Echols, N., Headd, J.J., Hung, L.W., Kapral, G.J., Grosse-Kunstleve, R.W., et al. (2010). PHENIX: a comprehensive Python-based system for macromolecular structure solution. Acta Crystallogr. D Biol. Crystallogr. *66*, 213–221.

Bernardes, A., Souza, P.C., Muniz, J.R., Ricci, C.G., Ayers, S.D., Parekh, N.M., Godoy, A.S., Trivella, D.B., Reinach, P., Webb, P., et al. (2013). Molecular mechanism of peroxisome proliferator-activated receptor alpha activation by WY14643: a new mode of ligand recognition and receptor stabilization. J. Mol. Biol. *425*, 2878–2893.

Bligh, E.G., and Dyer, W.J. (1959). A rapid method of total lipid extraction and purification. Can. J. Biochem. Physiol. *37*, 911–917.

Bollinger, J.G., Naika, G.S., Sadilek, M., and Gelb, M.H. (2013). LC/ESI-MS/MS detection of FAs by charge reversal derivatization with more than four orders of magnitude improvement in sensitivity. J. Lipid Res. *54*, 3523–3530.

Capelli, D., Cerchia, C., Montanari, R., Loiodice, F., Tortorella, P., Laghezza, A., Cervoni, L., Pochetti, G., and Lavecchia, A. (2016). Structural basis for PPAR partial or full activation revealed by a novel ligand binding mode. Sci. Rep. *6*, 34792.

Emsley, P., and Cowtan, K. (2004). Coot: model-building tools for molecular graphics. Acta Crystallogr. D Biol. Crystallogr. *60*, 2126–2132.

Evans, P.R., and Murshudov, G.N. (2013). How good are my data and what is the resolution? Acta Crystallogr. D Biol. Crystallogr. *69*, 1204–1214.

Kabsch, W. (2010). XDS. Acta Crystallogr. D Biol. Crystallogr. *66*, 125–132.

Kawasaki, M., Kambe, A., Yamamoto, Y., Arulmozhiraja, S., Ito, S., Nakagawa, Y., Tokiwa, H., Nakano, S., and Shimano, H. (2020). Elucidation of molecular mechanism of a selective PPARalpha modulator, pemafibrate, through combinational approaches of X-ray crystallography, Thermodynamic analysis, and first-principle calculations. Int. J. Mol. Sci. *21*, 361.

Laskowski, R.A., and Swindells, M.B. (2011). LigPlot+: multiple ligand-protein interaction diagrams for drug discovery. J. Chem. Inf. Model. *51*, 2778–2786.

Liu, Q., Dahmane, T., Zhang, Z., Assur, Z., Brasch, J., Shapiro, L., Mancia, F., and Hendrickson, W.A. (2012). Structures from anomalous diffraction of native biological macromolecules. Science *336*, 1033–1037.

McCoy, A.J., Grosse-Kunstleve, R.W., Adams, P.D., Winn, M.D., Storoni, L.C., and Read, R.J. (2007). Phaser crystallographic software. J. Appl. Crystallogr. *40*, 658–674.

Oyama, T., Toyota, K., Waku, T., Hirakawa, Y., Nagasawa, N., Kasuga, J.I., Hashimoto, Y., Miyachi, H., and Morikawa, K. (2009). Adaptability and selectivity of human peroxisome proliferator-activated receptor (PPAR) pan agonists revealed from crystal structures. Acta Crystallogr. D Biol. Crystallogr. *65*, 786–795.

Pettersen, E.F., Goddard, T.D., Huang, C.C., Couch, G.S., Greenblatt, D.M., Meng, E.C., and Ferrin, T.E. (2004). UCSF Chimera--a visualization system for exploratory research and analysis. J. Comput. Chem. *25*, 1605–1612.